2014

Dysferlin mediates the cytoprotective effects of TRAF2 following myocardial ischemia reperfusion injury

Huei-Ping Tzeng
Washington University School of Medicine in St. Louis

Sarah Evans
Washington University School of Medicine in St. Louis

Feng Gao
Washington University School of Medicine in St. Louis

Kari Chambers
Washington University School of Medicine in St. Louis

Veli K. Topkara
Washington University School of Medicine in St. Louis

See next page for additional authors

Dysferlin Mediates the Cytoprotective Effects of TRAF2 Following Myocardial Ischemia Reperfusion Injury

Huei-Ping Tzeng, Sarah Evans, Feng Gao, Kari Chambers, Veli K. Topkara, Natarajan Sivasubramanian, Philip M. Barger and Douglas L. Mann

J Am Heart Assoc. 2014;3:e000662; originally published February 26, 2014;
doi: 10.1161/JAHA.113.000662
The *Journal of the American Heart Association* is published by the American Heart Association, 7272 Greenville Avenue, Dallas, TX 75231
Online ISSN: 2047-9980

ORIGINAL RESEARCH

Dysferlin Mediates the Cytoprotective Effects of TRAF2 Following Myocardial Ischemia Reperfusion Injury

Huei-Ping Tzeng, PhD; Sarah Evans, PhD; Feng Gao, MD; Kari Chambers, PhD; Veli K. Topkara, MD; Natarajan Sivasubramanian, PhD; Philip M. Barger, MD; Douglas L. Mann, MD

***Background*—**We have demonstrated that tumor necrosis factor (TNF) receptor-associated factor 2 (TRAF2), a scaffolding protein common to TNF receptors 1 and 2, confers cytoprotection in the heart. However, the mechanisms for the cytoprotective effects of TRAF2 are not known.

***Methods/Results*—**Mice with cardiac-restricted overexpression of low levels of TRAF2 (MHC-TRAF2$_{LC}$) and a dominant negative TRAF2 (MHC-TRAF2$_{DN}$) were subjected to ischemia (30-minute) reperfusion (60-minute) injury (I/R), using a Langendorff apparatus. MHC-TRAF2$_{LC}$ mice were protected against I/R injury as shown by a significant ≈27% greater left ventricular (LV) developed pressure after I/R, whereas mice with impaired TRAF2 signaling had a significantly ≈38% lower LV developed pressure, a ≈41% greater creatine kinase (CK) release, and ≈52% greater Evans blue dye uptake after I/R, compared to LM. Transcriptional profiling of MHC-TRAF2$_{LC}$ and MHC-TRAF2$_{DN}$ mice identified a calcium-triggered exocytotic membrane repair protein, dysferlin, as a potential cytoprotective gene responsible for the cytoprotective effects of TRAF2. Mice lacking dysferlin had a significant ≈39% lower LV developed pressure, a ≈20% greater CK release, and ≈29% greater Evans blue dye uptake after I/R, compared to wild-type mice, thus phenocopying the response to tissue injury in the MHC-TRAF2$_{DN}$ mice. Moreover, breeding MHC-TRAF2$_{LC}$ onto a dysferlin-null background significantly attenuated the cytoprotective effects of TRAF2 after I/R injury.

***Conclusion*—**The study shows that dysferlin, a calcium-triggered exocytotic membrane repair protein, is required for the cytoprotective effects of TRAF2-mediated signaling after I/R injury. **(*J Am Heart Assoc*. 2014;3:e000662 doi: 10.1161/JAHA.113.000662)**

Key Words: cytoprotection • dysferlin • TNF receptor associated factor 2 • tumor necrosis factor

Myocardial reperfusion after a period of ischemia may be regarded as a "mixed blessing." That is, on the one hand, there is the clear-cut benefit that occurs as the result of recovery of heart muscle that attends reperfusion; however, on the other hand, there are also deleterious reperfusion-dependent effects that can be attributed to excessive activation of proinflammatory cytokines. Although excessive activation of proinflammatory cytokines may be overtly deleterious by producing left ventricular (LV) dysfunction and increased tissue destruction attributable to robust inflammatory response, there is increasing evidence that activation of proinflammatory cytokines may be beneficial by upregulating cytoprotective pathways, as well as by promoting tissue repair. Indeed, we and others have suggested that proinflammatory cytokines belonging to a phylogenetically conserved host defense system, collectively referred to as innate immunity, may be beneficial by upregulating cytoprotective pathways, as well as by promoting tissue repair.[1–4] Both gain- and loss-of-function studies have suggested an important role for tumor necrosis factor (TNF) with respect to mediating myocardial cytoprotection in vitro,[5] ex vivo,[2,4,6,7] as well as in vivo.[8–10] Moreover, TNF has been implicated as a mediator of classic ischemic preconditioning, through a signal transducer and activator of transcription 3–dependent pathway (SAFE pathway).[4] We have shown, through a variety of experimental approaches, that signaling through the type 1 (TNFR1) and type 2 (TNFR2) TNF receptors is sufficient to mimic the effects of TNF in vitro and ex vivo.[5,11] Although it is conceivable that TNFR1 and TNFR2 activate disparate cytoprotective signal transduction pathways, the most parsimonious explanation is that TNFR1 and TNFR2 transduce a common cytoprotective repertoire in the heart. Noting that the intracellular scaffolding protein, TNFR-associated factor 2 (TRAF2) was common to

From the Center for Cardiovascular Research, Division of Cardiology, Department of Medicine, Washington University School of Medicine, St. Louis, MO (H.-P.T., S.E., K.C., V.K.T., P.M.B., D.L.M.); Winters Center for Heart Failure Research Section of Cardiology, Baylor College of Medicine, Houston, TX (F.G., N.S.).

Correspondence to: Douglas L. Mann, MD, Division of Cardiology, 660 S Euclid Ave, Campus Box 8086, St. Louis, MO 63110. E-mail: dmann@dom.wustl.edu

Received December 13, 2013; accepted January 28, 2014.

both TNFR1 and TNFR2, and recognizing that TRAF2 mediates cytoprotection in nonmyocyte cell types,[12] we reasoned that the cytoprotective effects of TNF in the heart were mediated, at least in part, through TRAF2. To this end, we generated lines of mice with low levels of TRAF2 expression in the heart (MHC-TRAF2$_{LC}$) and demonstrated that these mice had significantly improved LV functional recovery and significantly less LV tissue injury after ischemia-reperfusion (I/R) injury, when compared to littermate (LM) control mice.[11]

To extend our initial observations with respect to the cytoprotective role of TRAF2 in the heart, here we generate lines of mice with a cardiac-restricted dominant negative form of TRAF2 (MHC-TRAF2$_{DN}$). Notably, hearts from MHC-TRAF2$_{DN}$ mice demonstrated an I/R injury-induced phenotype that was opposite to the MHC-TRAF2$_{LC}$ mice, namely, increased membrane permeability, increased creatine kinase (CK) release, and significantly worse LV functional recovery after reperfusion. Transcriptional profiling of MHC-TRAF2$_{LC}$ and MHC-TRAF2$_{DN}$ mice and subsequent functional studies in mice identified dysferlin, a calcium-triggered exocytotic membrane repair protein, as a novel cytoprotective gene that mediates the cytoprotective effects of TRAF2-mediated signaling in the mammalian heart.

Methods

Generation and Characterization of Transgenic and Knockout Mice

MHC-TRAF2$_{DN}$ Transgenic Mice

Mice with cardiac-restricted expression of dominant negative TRAF2 (MHC-TRAF2$_{DN}$) were generated using a dominant negative TRAF2 construct (a generous gift from Dr Yongwon Choi[13]), in which the N-terminal domain of TRAF2 (TRAF2$_{241-501}$) lacking the N-terminal ring and zinc fingers essential for TRAF2-mediated nuclear factor kappa B (NF-κB)- and c-Jun N-terminal kinase (JNK)-mediated signaling was deleted. Briefly, the TRAF2$_{\Delta 241-501}$ mutant construct was inserted behind the myosin heavy chain (αMHC) promoter, which was obtained from Dr Jeff Robbins. The TRAF2$_{DN}$ transgene constructs were injected into single-cell embryos of Friend virus B (FVB) mice at the Transgenic Core Facility at Baylor College of Medicine, as previously described.[11] Founder lines were identified by Southern blotting, as described above.[11] Age-matched LM mice that lacked the transgene were used as appropriate controls. Hemizygous MHC-TRAF2$_{DN}$ mouse lines were characterized at 12 weeks of age using standard morphological and histological analyses, as well as two-dimensional (2D)-targeted M-mode echocardiography (Echo), as previously described.[11] Further characterization of MHC-TRAF2$_{DN}$ mice was performed by examining activation of NF-κB in nuclear extracts obtained from hearts of 12-week naïve MHC-TRAF2$_{DN}$ and LM control mice. Electrophoretic mobility shift assays (EMSAs) were performed, as previously described,[11] using an NF-κB oligonucleotide consensus sequence (5′-AGT TGA GGG GAC TTT CCC AGG C-3′; Santa Cruz Biotechnology, Santa Cruz, CA). Specificity of binding was determined by competition with a 20× molar excess of the respective unlabeled oligonucleotide. JNK activation was determined in LM control and MHC-TRAF2$_{DN}$ hearts at 12 weeks of age by Western blot analysis, using rabbit anti-JNK (Catalog No. 9252; Cell Signaling Technology, Danvers, MA) and rabbit anti-phospho-JNK antibody (Catalog No. 9251 from Cell Signaling Technology).

MHC-TRAF2$_{LC}$ Transgenic Mice

The hemizygous line of transgenic (Tg) mice with cardiac-restricted overexpression of low levels of TRAF2 (referred to as MHC-TRAF2$_{LC}$) have been described elsewhere in detail (FVB background).[11] Briefly, MHC-TRAF2$_{LC}$ hearts have improved LV functional recovery, decreased myocardial CK release, and decreased uptake of Evans blue dye after I/R injury ex vivo, when compared to LM controls.[11]

Dysferlin-Null Mice

Dysferlin-null mice (129-Dysf^{tm1Kcam}/J [dysferlin$^{-/-}$]),[14] maintained on a 129 background, were purchased from The Jackson Laboratory (dysferlin$^{-/-}$; Stock No. 006830; Bar Harbor, ME). The lines of 129S1/SvImJ (129) wild-type (WT) mice that were used as the appropriate controls (http://jaxmice.jax.org/strain/002448.html) were also purchased from The Jackson Laboratory (129; Stock No. 0024480). Dysferlin$^{-/-}$ mice were characterized at 12 weeks of age using standard morphological and histological analyses, as well as 2D-targeted M-mode ECG, as previously described.[11] LV function was assessed ex vivo in 12-week dysferlin$^{-/-}$ and WT mouse hearts using a buffer-perfused Langendorff apparatus, as previously described.[15]

MHC-TRAF2$_{LC}$/Dysferlin-Null Mice

MHC-TRAF2$_{LC}$ were outcrossed with dysferlin$^{-/-}$ mice to produce F1 lines of MHC-TRAF2$_{LC}$/dysferlin$^{-/+}$ mice. F1 MHC-TRAF2$_{LC}$/dysferlin$^{-/+}$ mice were back-crossed with dysferlin$^{-/-}$ mice to generate MHC-TRAF2$_{LC}$/dysferlin$^{-/-}$ mice or with 129 mice to generate WT/dysferlin$^{+/+}$ control mice. F2 lines of mice were used for all experiments.

For all studies reported herein, we used 12- to 14-week-old male mice. Animals were housed under standard environmental conditions and fed standard chow and tap water ad libitum. All experiments were approved by the Institutional Animal Care and Use Committees at the Baylor College of Medicine and Washington University School of Medicine and

were conducted in accord with the guidelines of the Baylor College of Medicine and Washington University School of Medicine Animal Care and Research Advisory Committee and the rules governing animal use, as published by the National Institutes of Health (NIH; Bethesda, MD).

I/R Injury

Hearts from MHC-TRAF2$_{DN}$, MHC-TRAF2$_{LC}$, dysferlin$^{-/-}$, and MHC-TRAF2$_{LC}$/dysferlin$^{-/-}$ mice and their respective LM and/or WT controls were isolated and perfused in the Langendorff mode, as previously described.[11] In brief, isolated hearts were perfused at a constant pressure of 70 mm Hg with modified Krebs-Henseleit buffer containing (in mmol) 118 NaCl, 24 $NaHCO_3$, 4.7 KCl, 1.2 KH_2PO_4, 1.2 $MgSO_4$, 2.2 $CaCl_2$, 10 glucose, and 2 pyruvate, equilibrated with 95% O_2-5% CO_2 to yield a pH of 7.4 (37°C). A hand-made balloon was inserted into the LV and connected to a pressure transducer (ML844; ADInstruments, Colorado Springs, CO). The balloon was inflated with water to adjust LV end-diastolic pressure (LVEDP) at 5 to 10 mm Hg. All hearts were paced at 420 bpm with pacing electrodes placed on the right atrium. After a 20-minute stabilization period, hearts were subjected to no-flow ischemia (t=0 minutes) for 30 minutes, followed by reperfusion (t=30 minutes) for up to 60 minutes (t=90 minutes). Functional data were recorded at 1 kHz on a data acquisition system (PowerLab; ADInstruments). LV developed pressure (LVDP) was calculated as the difference between peak systolic pressure and LVEDP, and the resulting LV functional recovery data are expressed as the percentage of LVDP at baseline.

Assessment of Cardiac Myocyte Injury After I/R Injury

To assess the effects of I/R injury on cardiac myocyte injury in MHC-TRAF2$_{DN}$, MHC-TRAF2$_{LC}$, dysferlin$^{-/-}$, MHC-TRAF2$_{LC}$/dysferlin$^{-/-}$, and WT control hearts, we assessed CK release in the effluent 30 minutes after reperfusion, as previously described.[11] Data are expressed as units per gram of cardiac tissue. Because triphenyltetrazolium chloride staining may underestimate the true extent of tissue injury within the first 3 hours of cardiac injury,[16] we used Evans blue dye uptake to assess the degree of myocardial tissue injury after I/R injury, as previously described.[11] Briefly, Evans blue dye crosses into cells with permeable membranes and accumulates in myofibrils, where it emits red autofluorescence when examined using fluorescence microscopy. Fluorescence microscopy (×200) was performed using a filter set with an excitation of 510 to 560 nm and an emission of 590 nm in order to assess the amount of Evans blue dye uptake in the myocardium at baseline and after I/R injury. Hearts were examined at the level of the papillary muscle, using a total of 30 microscopic fields per heart. Data are expressed as the percent area of the myocardium with red fluorescence.

Transcriptional Profiling in MHC-TRAF2$_{LC}$ and MHC-TRAF2$_{DN}$ Hearts

Total RNA was extracted from hearts of MHC-TRAF2$_{LC}$, MHC-TRAF2$_{DN}$, and LM control mice using TRIzol reagent (Invitrogen, Carlsbad, CA), according to the manufacturer's instructions. Gene expression analysis was performed using the Sentrix BeadChip and BeadStation system from Illumina, Inc (San Diego, CA). RNA was further processed and hybridized to a Mouse Ref-6.1.1 BeadChip array (Illumina). The mouse Ref-6 BeadChips contain sequences representing ≈46 000 curated genes and expressed sequence tags (ESTs). After scanning the probe array, the resulting image was analyzed using BeadStudio software (Illumina). Samples were normalized using a cubic spline procedure.

Differentially expressed genes between MHC-TRAF2$_{LC}$ and MHC-TRAF2$_{DN}$ and LM controls were determined using an ANOVA test with contrasts using Partek GS (Partek, St. Louis, MO) using an unadjusted P value <0.05 and a fold change of 1.2 or greater. Agglomerative hierarchical clustering (combination of two rows/columns or clusters at each step of the procedure) was also performed using Partek GS. Euclidean distance was used to measure dissimilarity (the distance between two rows or columns), and average linkage (the average distance between all pairs of objects in two different clusters) was used as the measure of distance between two clusters. An analysis of gene expression in relation to cellular components was performed using the Database for Annotation Visualization and Integrated Discovery (http://david.abcc.ncifcrf.gov/),[17] according to the classification of cellular components assigned by the Gene Ontology (GO) Consortium.

Dysferlin mRNA and Protein Expression in MHC-TRAF2$_{LC}$ and MHC-TRAF2$_{DN}$ Hearts

Dysferlin mRNA levels were determined in 12-week hearts from MHC-TRAF2$_{LC}$, MHC-TRAF2$_{DN}$, and LM control mice by real-time quantitative polymerase chain reaction (RT-qPCR), using an ABI 7500 Fast Real-Time quantitative PCR System (Applied Biosystems, Foster City, CA). Two micrograms of total RNA was reverse transcribed into cDNA using the High-Capacity cDNA Reverse Transcription Kit (Applied Biosystems). cDNAs were amplied for 18S rRNA (Part No.: 4333760F) and dysferlin (Assay ID No.: Mm00458042_m1) using the TaqMan gene expression assay (Applied Biosystems), and the final results represent the fold change relative to LM controls using the ΔΔCt method with normalization to 18s expression.

Dysferlin protein levels were determined in membrane preparations obtained from 12-week-old MHC-TRAF2$_{LC}$, MHC-

$TRAF2_{DN}$, and LM control mice. Briefly, LV tissue was homogenized in isotonic sucrose buffer containing (in mmol/L): 20.0 Tris-HCl, 250.0 sucrose, 1 Na_3VO_4, 2.0 $MgCl_2$, 2.0 EDTA, 0.5 EGTA, 2.0 phenylmathanesulfonyl fluoride, and 1.0 dithiothreitol and 0.02% (vol/vol) protease inhibitor cocktail (pH 7.4). Homogenates were centrifuged at 100 000*g* for 60 minutes at 4°C to separate the particulate fraction from the cytosolic fraction, and the resulting pellet was resonicated in sucrose buffer containing 0.1% Triton X-100 and centrifuged at 100 000*g* for 30 minutes at 4°C. Equivalent amounts (50 μg) of supernatant protein were separated on a 10% SDS-PAGE and transferred to nitrocellulose membranes. Western blot analysis was performed using rabbit anti-dysferlin (1:1000; Epitomics, Burlingame, CA), followed by a peroxidase-labeled secondary antibody (1:3000; Cell Signaling). Antigen-antibody complexes were visualized by enhanced chemiluminescence (ECL; Amersham Pharmacia Biotech, Piscataway, NJ). Membranes were incubated at 70°C for 10 minutes in stripping buffer and then reprobed for rabbit anti-calsequestrin (1:1000; Abcam, Cambridge, MA). Original films were exposed to ECL (Hyperfilm™, ECL™; Amersham Pharmacia Biotech), and band density was determined (in arbitrary units) using the software, ImageJ (NIH). Dysferlin protein levels were normalized by calsequestrin levels to account for any potential loading differences.

NF-κB-Induced Activation of Dysferlin Gene Expression

Previous studies from this laboratory have suggested that TNF-TRAF2-mediated activation of NF-κB is responsible for provoking cytoprotective responses in the heart after I/R injury.[11] To determine whether NF-κB was involved in upregulation of dysferlin in MHC-$TRAF2_{LC}$ mouse hearts, we performed a chromatin immunoprecipitation (ChIP) assay using the EZ-ChIP Assay Kit (Millipore, Temecula, CA), following the manufacturer's instructions. Briefly, mouse hearts were minced and incubated in PBS containing 1% formaldehyde at room temperature for 10 minutes to cross-link proteins to DNA. Cross-linking was stopped by adding 2.5 mol/L glycine to a final concentration of 0.125 mol/L. Tissue was then washed twice in cold PBS, homogenized in 2 mL PBS containing Protease Inhibitor Cocktail II, pelleted, and resuspended in 1 mL SDS lysis buffer containing Protease Inhibitor Cocktail II. Chromatin was sonicated to shear cross-linked DNA to ≈200 to 1000 bp in length. Sheared chromatin was precleared with Protein G Agarose for 1 hour at 4°C with rotation. After pelleting agarose, 1% volume of each sample was removed to use as input. The remaining chromatin was immunoprecipitated with antibodies against NF-κB family members (RelB: sc-226, Santa Cruz; p50: ab7971, Abcam; p65: No. 8242, Cell Signaling; p52: ab7972, Abcam) or control antibodies overnight at 4°C with rotation. Protein G Agarose was then added to protein/DNA complexes at 4°C for 1 hour. Agarose was pelleted and washed sequentially with low-salt buffer, high-salt buffer, LiCl wash buffer, and Tris-EDTA buffer. Protein/DNA cross-links were reversed by incubating samples at 65°C overnight. Chromatin was then digested with RNase at 37°C for 30 minutes and with proteinase K at 45°C for 2 hours. DNA was purified with spin filters provided with the kit. PCR was performed with 4 μL of immunoprecipitated DNA using the following primers: forward, 5′CATATAAGCCTGTGCCCTCATAAGAAC 3′; reverse, 5′GGATGC TGTAGATAGACGACTGAGAA3′. Primers were chosen based on a kB site in the dysferlin variant 1 promoter predicted by the TFSearch (http://www.cbrc.jp/research/db/TFSEARCH.html), Promo (http://alggen.lsi.upc.es/cgi-bin/promo_v3/promo/promoinit.cgi?dirDB=TF_8.3), and TFBIND (http://tfbind.hgc.jp/) programs.

To determine whether I/R injury resulted in differential localization of dysferlin in cardiac myocytes from MHC-$TRAF_{LC}$ mouse hearts, compared to LM controls, we performed immunohistochemical (IHC) staining at baseline and after 60 minutes of I/R injury. Briefly, hearts were subjected to the I/R protocol exactly as described above and were then perfuse fixed with Z-fix (Anatech, Battle Creek, MI). Antigen retrieval was performed by placing slides in retrieval buffer (180 μmol/L citric acid, 820 μmol/L sodium citrate) and heating in a microwave 3× for 4 minutes. Tissue was then permeabilized using 1× TBS/0.1% Triton X-100 for 20 minutes at room temperature. After permeabilization, tissue was blocked in a buffer containing 10× blocking reagent (Roche, Indianapolis, IN), 9 mL FCS, and 27 maleate buffer (100 mmol/L maleic acid, 150 mmol/L NaCl; pH 7.5) for 30 minutes at room temperature. A primary rabbit anti-dysferlin monoclonal antibody (Romeo; Epitomics, Burlingame, CA) was applied overnight at 4°C (1:50 dilution in blocking buffer). Slides were washed with 1× TBS/0.1% Tween 3× 5 minutes each and labeled with a red fluorescence-conjugated anti-rabbit secondary antibody (Alexa Fluor 647; Life Technologies, Carlsbad, CA) for 1 hour at room temperature (1:500 dilution in blocking buffer). Slides were washed with TBS/0.1% Tween, mounted with Vectashield containing 4',6-diamidino-2-phenylindole (DAPI; Vector Laboratories, Burlingame, CA), and imaged using a Zeiss confocal (LSM 700 Laser Scanning Confocal; Carl Zeiss GmbH, Jena, Germany) microscope using DAPI and Alexa Fluor 647 filters.

Statistical Analysis

Data are expressed as mean±SEM. Two-way repeated-measures ANOVA was used to test for differences in percent LVDP between groups as a function of time after I/R injury between groups. Post-hoc ANOVA testing was performed, where appropriate, using Fisher's least significant difference

test.[18] CK release, the area of the myocardium (%) with Evans blue uptake after I/R injury, dysferlin mRNA and protein levels, and heart weight/body weight ratios were examined using a nonpaired *t* test. All data were tested for normality before performing parametric testing. Significant differences were said to exist at $P<0.05$.

Results

Generation and Characterization of Tg and Knockout Mice

MHC-TRAF2$_{DN}$ Tg mice

We obtained five founder lines of mice, harboring 1, 10, 15, 25, and 30 copies of the cardiac-restricted TRAF2$_{DN}$ transgene. For the present study, we selected the MHC-TRAF$_{DN}$ line harboring 30 copies of the transgene (MHC-TRAF2$_{DN}$). MHC-TRAF2$_{DN}$ mice were born with the expected Mendelian frequency and developed normally. MHC-TRAF2$_{DN}$ mice lacked a cardiac phenotype at 12 weeks of age, as assessed by gross morphology and hematoxylin and eosin (H&E) staining (Figure 1A), as well as by assessment of heart weight/body weight ratio (Figure 1B), and 2D ECG assessment of LV structure (Figure 2A through 2C). Further characterization of 12-week-old mice showed no differences in LV function in MHC-TRAF2$_{DN}$, compared with LM controls, when assessed in vivo by 2D ECG or ex vivo by buffer-perfused Langendorff apparatus (Figure 2D through 2G). To further characterize MHC-TRAF2$_{DN}$ mice, we examined NF-κB and JNK activity in 12-week-old LM and MHC-TRAF2$_{DN}$ mice. As expected, neither NF-κB nor JNK were activated in naïve MHC-TRAF2$_{DN}$ mouse hearts. EMSAs from hearts of mice with targeted overexpression of TRAF2, which were used as positive controls, had activation of NF-κB, as we have reported previously.[19]

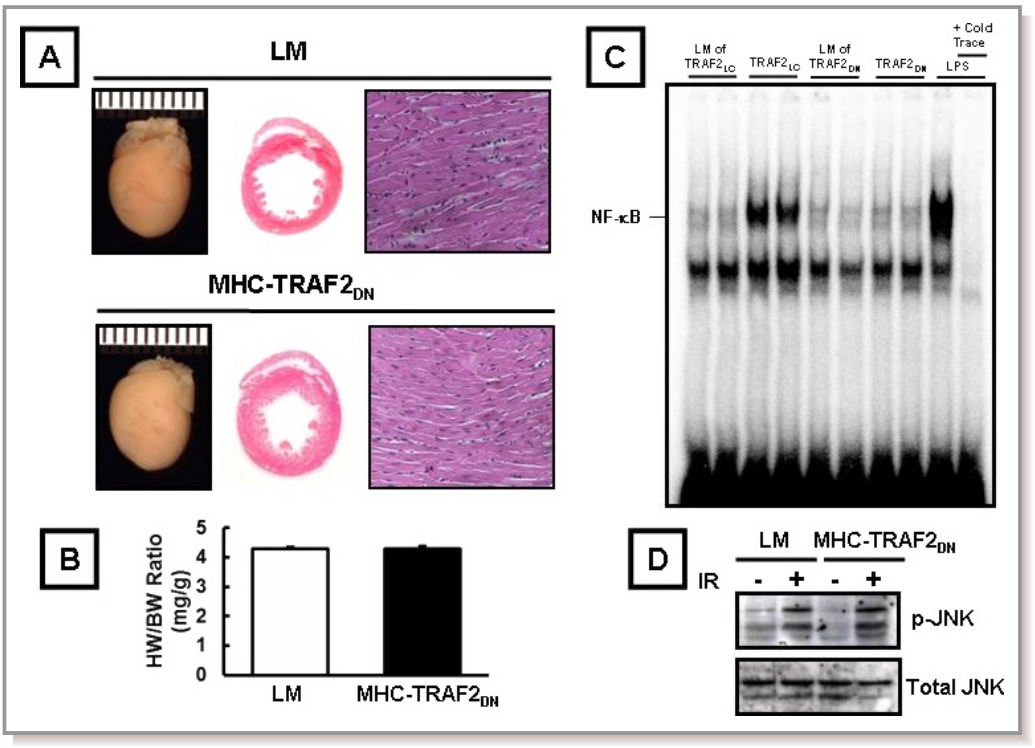

Figure 1. Characterization of transgenic mice expressing dominant negative TRAF2 (MHC-TRAF2$_{DN}$), compared to littermate (LM) control mice. A, Representative photographs of 12-week MHC-TRAF2$_{DN}$ transgenic and LM control hearts, hematoxylin and eosin–strained cross-sections at the level of the papillary muscle, and representative hematoxylin and eosin–stained cross-sections at the level of the papillary muscles (×400). B, Heart weight/body weight ratio (n=6/group). C, Left panel: Electromobility shift assay (EMSA) of NF-κB activation in nuclear extracts from LM, MHC-TRAF2$_{LC}$ (positive control), MHC-TRAF2$_{DN}$, and lipopolysaccharide (LPS)-stimulated hearts (20 mg/kg intraperitoneally for 1 hour). Specificity of DNA-protein-binding nuclear extracts was determined using a 20× molar excess of the respective unlabeled oligonucleotide. D, JNK activation assay in LM and TRAF2$_{DN}$ hearts (12 weeks) at baseline and after I/R injury. BW indicates body weight; HW, heart weight; I/R, ischemia-reperfusion; JNK, c-Jun N-terminal kinase; MHC, myosin heavy chain; NF-κB, nuclear factor kappa B; TRAF2, tumor necrosis factor receptor-associated factor 2.

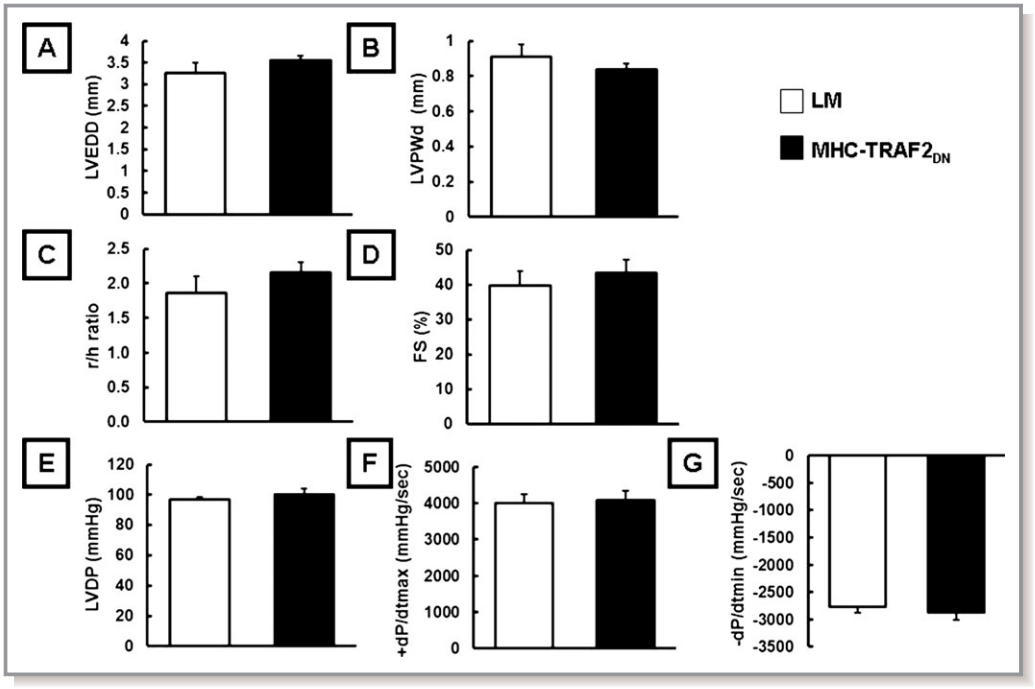

Figure 2. LV structure and function in MHC-TRAF2$_{DN}$ mice. 2D-targeted echocardiography was used in 12-week MHC-TRAF2$_{DN}$ transgenic and littermate (LM) control mice to determine (A) LV end-diastolic dimension (LVEDD), (B) LV posterior wall diameter (LVPWd), (C) ratio of LV radius to LV wall thickness (r/h), and (D) percent LV fractional shortening (% FS) (n=5 control group; n=6 transgenic mice). Buffer-perfused Langendorff apparatus was used to determine (E) percent LV developed pressure (LVDP), (F) LV +dP/d*t*, and (G) LV −dP/d*t* in 12-week MHC-TRAF2$_{DN}$ transgenic and LM hearts (n=6/group). LV indicates left ventricle; TRAF2, tumor necrosis factor receptor-associated factor 2.

Effects of Cardiac-Restricted Overexpression of Dominant Negative TRAF2 After I/R Injury

To determine the effects of loss of TRAF2-mediated signaling after I/R injury, we subjected MHC-TRAF2$_{DN}$ mice to 30 minutes of no-flow ischemia, followed by 60 minutes of reperfusion. The salient finding shown by Figure 3A is that hearts from MHC-TRAF2$_{DN}$ mice had significantly worse LV functional recovery at 10 to 60 minutes (P<0.05/time point) after reperfusion, when compared to the LM control mice. To determine whether the decreased functional recovery of MHC-TRAF2$_{DN}$ mice was the result of increased myocyte injury, we measured CK release and Evans blue dye uptake 30 minutes after reperfusion. As shown in Figure 3B, there was a significant (P<0.05) 1.4-fold increase in CK release after I/R injury in MHC-TRAF2$_{DN}$ hearts, when compared to LM control hearts. Consistent with these findings, there was a significant (P<0.05) increase in Evans blue dye uptake in MHC-TRAF2$_{DN}$ mouse hearts, as depicted by the representative fluorescence photomicrographs shown in Figure 3C and the group data summarized in Figure 3D. In contrast, hearts from MHC-TRAF2$_{LC}$ mice that were subjected to I/R injury demonstrated significantly improved LV functional recovery 10 to 60 minutes (P<0.05/time) after IR injury, compared to LM controls, consistent with our earlier observations.[11] Viewed together, these results suggest that low levels of myocardial TRAF2 are sufficient to protect cardiac myocytes against I/R injury, whereas loss of TRAF2-mediated signaling in cardiac myocytes leads to increased cardiac myocyte injury and decreased functional recovery after I/R injury.

Transcriptional Profiling in MHC-TRAF2$_{LC}$ and MHC-TRAF2$_{DN}$ Hearts

To explore the potential mechanisms responsible for the cytoprotective effects of TRAF2 in the adult heart, we performed transcriptional profiling in 12-week-old naïve LM, MHC-TRAF2$_{LC}$, and MHC-TRAF2$_{DN}$ hearts. Transcriptional profiling revealed that there were 1059 upregulated genes and 1199 downregulated genes in MHC-TRAF2$_{LC}$ hearts, in comparison to LM controls, whereas MHC-TRAF2$_{DN}$ hearts had 965 upregulated genes and 1089 downregulated genes, in comparison to LM controls (Figure 4A and 4B). Agglomerative hierarchical clustering of these transcriptional profiles showed that gene expression profiles in the MHC-TRAF2$_{LC}$ and MHC-TRAF2$_{DN}$ mouse hearts clustered differently than those in LM control hearts (Figure 5), suggesting that gain and loss of TRAF2 signaling in the heart results in discordant

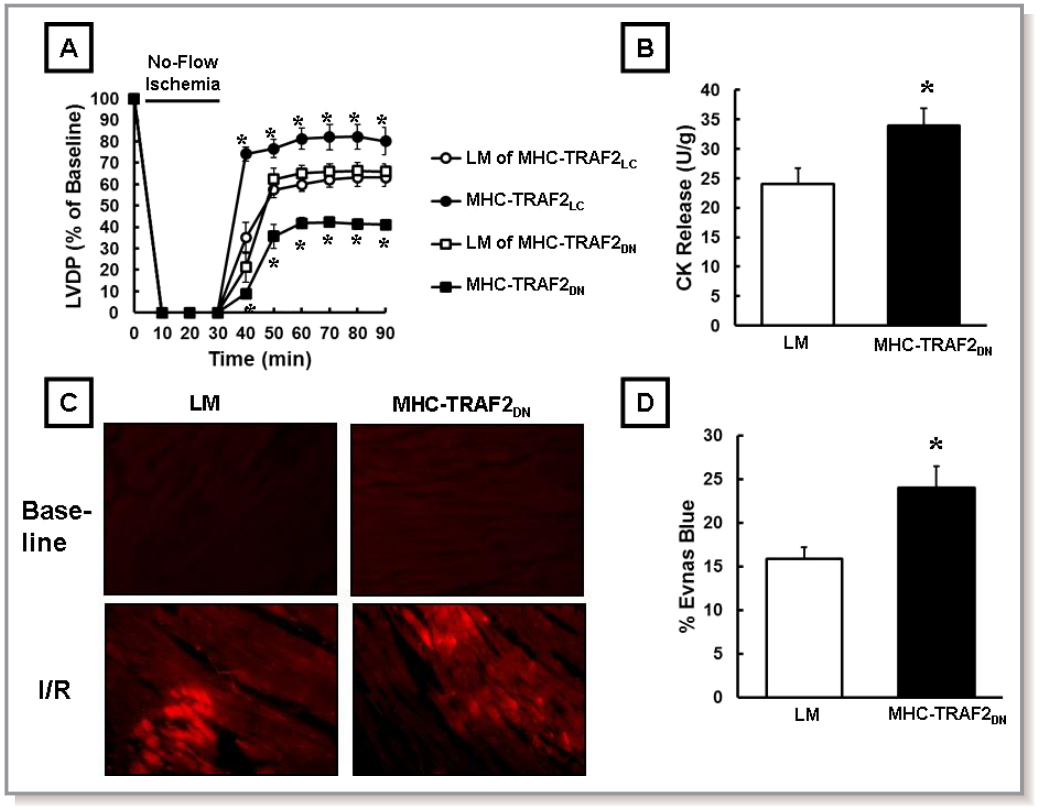

Figure 3. Effects of I/R injury on transgenic mice expressing low levels of TRAF2 (MHC-TRAF2$_{LC}$) or dominant negative TRAF2 (MHC-TRAF2$_{DN}$) and their respective littermate (LM) controls. A, Percent of left ventricular developed pressure after I/R injury (n=6/group). B, CK release in the effluent 30 minutes after I/R injury in MHC-TRAF2$_{DN}$ and LM controls (n=7/group). C, Representative images of Evans blue dye uptake. Red coloration indicates uptake of Evans blue dye into necrotic/permeable cardiac myocytes. D, Group data for Evans blue uptake (n=7/group). *P<0.05, compared to LM controls. CK indicates creatine kinase; I/R, ischemia-reperfusion; LVDP, left ventricle developed pressure; TRAF2, tumor necrosis factor receptor-associated factor 2.

changes in gene expression relative to WT levels of TRAF2 signaling. Moreover, gene expression profiles of MHC-TRAF2$_{DN}$ hearts clustered with LM control hearts. Based upon the functional studies shown in Figure 3, which suggested that gain and loss of function of TRAF2 signaling led, respectively, to improved and worsened responses to I/R injury, as well as the transcriptional profiling studies, which suggested that MHC-TRAF2$_{DN}$ and the MHC-TRAF2$_{LC}$ mouse hearts had distinct gene profiles, we focused our search for potential candidate cytoprotective genes on those genes whose expression level (relative to LM) was discordant (opposite) in MHC-TRAF2$_{DN}$ and in the MHC-TRAF2$_{LC}$ mouse hearts. Figure 4 shows that there were 94 discordant genes that were upregulated in MHC-TRAF2$_{LC}$ mice and downregulated in MHC-TRAF2$_{DN}$ mice (referred to as "Up/Down"; Figure 4A), and there were 110 discordant genes that were downregulated in MHC-TRAF2$_{LC}$ mice and upregulated in MHC-TRAF2$_{DN}$ mice (referred to as "Down/Up"; Figure 4B). Of the 94 discordant genes identified in the Up/Down group, there were 25 expressed sequence tags (ESTs) and 69 known genes. Of the 110 discordant genes in the Down/Up group, there were 31 ESTs and 79 known genes (see Table 1). We then performed a GO analysis of cellular components on the 148 genes identified in the Up/Down and Down/Up groups. As shown in Figure 4C, the cellular components that were enriched (greatest to least) included cytoplasm (P=0.047$\times 10^{-4}$), mitochondrion (P=0.025$\times 10^{-4}$), plasma membrane (P=0.047), cytoskeleton (P=0.052), endosome (P=0.014), and nucleus (P=0.09). Given that our results implicated TRAF2 signaling with preservation of membrane integrity after I/R injury (Figure 3C and 3D), as well as previous in vitro studies from this laboratory, which demonstrated that TNFR1- and TNFR2-mediated signaling preserved sarcolemmal integrity after hypoxia reoxygenation injury,[5] we focused our search on genes in the plasma membrane gene cluster. Table 2 depicts those discordantly regulated genes in MHC-TRAF2$_{DN}$ and MHC-TRAF2$_{LC}$ mouse hearts that were identified in the plasma membrane gene cluster. An expanded

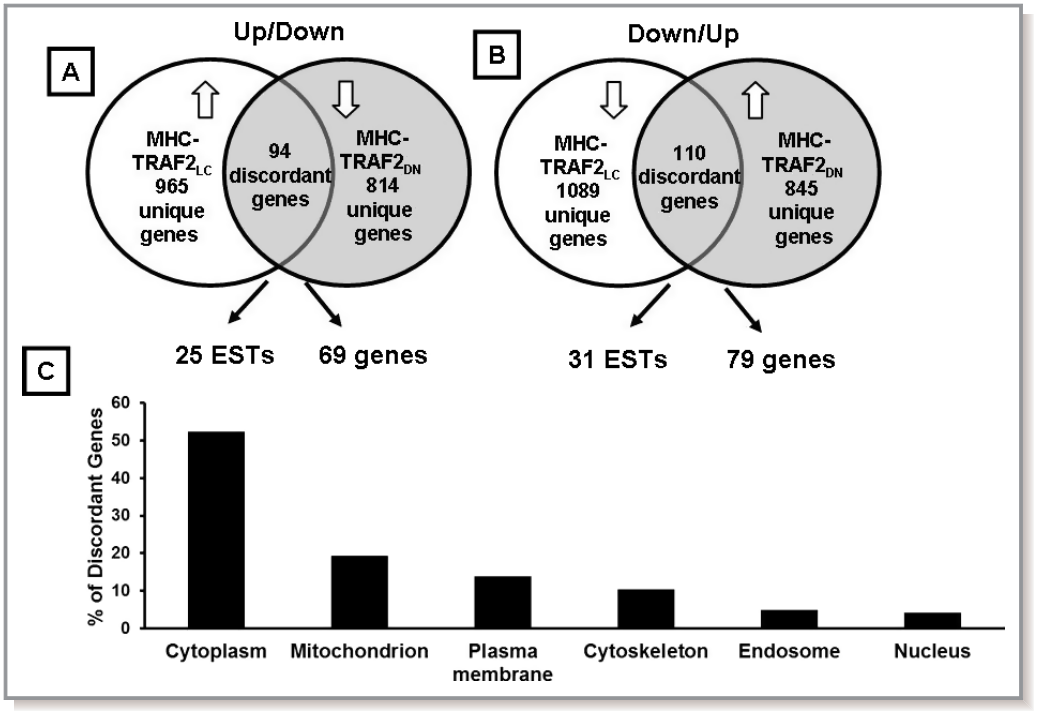

Figure 4. Transcriptional profiles of MHC-TRAF2$_{LC}$ and MHC-TRAF2$_{DN}$ hearts. A, Venn diagram of significantly (P<0.05) upregulated transcripts in MHC-TRAF2$_{LC}$ (1086) and downregulated transcripts in MHC-TRAF2$_{DN}$ (833), compared to LM controls (Up/Down). B, Venn diagram of significantly (P<0.05) downregulated transcripts in MHC-TRAF2$_{LC}$ (1103) and upregulated in MHC-TRAF2$_{DN}$ (844), compared to LM controls (Down/Up). C, Gene ontology cellular component analysis of the discordant genes (Up/Down and Down/Up transcripts). LM indicates littermate; TRAF2, tumor necrosis factor receptor-associated factor 2.

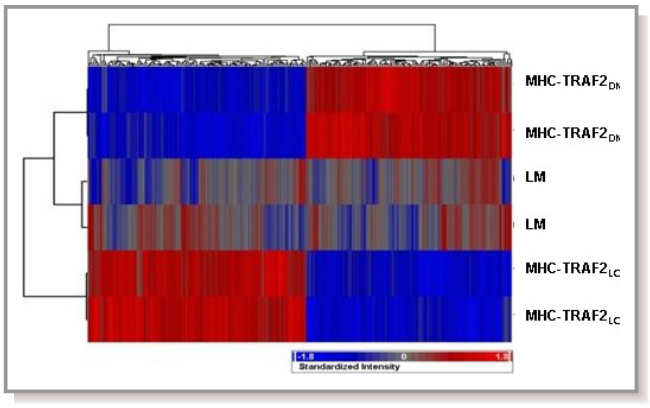

Figure 5. Transcriptional profiling of MHC-TRAF2$_{LC}$ and MHC-TRAF2$_{DN}$ hearts. Hierarchical clustering of significant changes in gene expression in 12-week MHC-TRAF2$_{LC}$ and MHC-TRAF2$_{DN}$ control mice, relative to LM controls. LM indicates littermate; TRAF2, tumor necrosis factor receptor-associated factor 2.

version of this table that includes gene function (neXProt [http://www.nextprot.org/db/]) and the GO biological processes for each gene (http://www.geneontology.org) is presented in Table 3. Inspection of Table 3 reveals that there were clusters of genes involved in the cytoskeleton/integrins (ENAH, ITGB5, VASP, RALB, ITGB1, DST, and SYNC), ion channels (KCNH2, KCNB1), energetics (ATP1B1), cell death (FKBP8, RHOB, and MFGE8), membrane trafficking (DYS, MSN, RAB11A, and RAB3A), and cell signaling (PPP1R9B, PLXND, EPS15, CAMK2N1, ATF6B, ASAH2, and CISH). Of these potential candidate genes, dysferlin was of particular interest because of its role in maintaining sarcolemmal integrity through exocytotic membrane "patch" repair.[20] We therefore focused on the potential role of dysferlin in TRAF2-mediated cytoprotection.

To confirm results with respect to the dysferlin gene array transcriptional profiling studies, we performed RT-qPCR and Western blot analysis in hearts of LM, MHC-TRAF2$_{DN}$, and MHC-TRAF2$_{LC}$ mouse hearts. As shown in Figure 6A, mRNA levels of dysferlin were significantly increased (P<0.05) in MHC-TRAF2$_{LC}$ hearts, compared to LM controls. Although there was a decrease in dysferlin mRNA in MHC-TRAF2$_{DN}$ hearts, when compared to LM controls, this change was not significantly statistically (P=0.09). Importantly, Western blot analysis demonstrated that membrane protein levels of dysferlin were 1.8-fold upregulated (P<0.0001) in MHC-TRAF2$_{LC}$ hearts and downregulated 0.7-fold (P<0.05) in MHC-TRAF2$_{DN}$ hearts, compared to respective LM controls (Figure 6B). Accordingly, we focused subsequent studies on

Table 1. Discordant Genes in $TRAF2_{LC}$ and $TRAF2_{DN}$ Mice

Gene Symbol	Gene Name	*P* Value	Fold Change	*P* Value	Fold Change
Up/down		$TRAF2_{LC}$ versus LM	$TRAF2_{LC}$ versus LM	$TRAF2_{DN}$ versus LM	$TRAF2_{DN}$ versus LM
TSC22D4	TSC22 domain family, member 4	7.03E-05	4.41	3.95E-02	−1.18
CCND2	Cyclin D2	1.56E-03	1.94	2.58E-02	−1.28
PSMD8	Proteasome (prosome, macropain) 26S subunit, non-ATPase, 8	9.57E-03	1.72	1.86E-02	−1.53
CKB	Creatine kinase, brain	1.11E-03	1.67	8.51E-04	−1.76
SYNPO2L	Synaptopodin 2-like	3.21E-03	1.67	4.73E-02	−1.21
MLLT11	Myeloid/lymphoid or mixed-lineage leukemia (trithorax homolog, *Drosophila*); translocated to, 11	1.12E-03	1.61	1.42E-02	−1.22
PLXNB2	Plexin B2	3.01E-04	1.60	8.14E-03	−1.16
ACTA2	Actin, alpha 2, smooth muscle, aorta	2.43E-02	1.51	4.68E-03	−2.10
VASP	Vasodilator-stimulated phosphoprotein	8.38E-03	1.50	4.49E-02	−1.24
SERPINH1	Serpin peptidase inhibitor, clade H (heat shock protein 47), member 1, (collagen binding protein 1)	9.25E-03	1.49	4.94E-02	−1.24
MASP1	Mannan-binding lectin serine peptidase 1 (C4/C2 activating component of Ra-reactive factor)	2.29E-03	1.44	4.52E-03	−1.33
STXBP1	Syntaxin-binding protein 1	2.37E-02	1.43	3.86E-02	−1.35
PPP1R9B	Protein phosphatase 1, regulatory (inhibitor) subunit 9B	2.66E-03	1.37	2.16E-02	−1.16
TMEM63C	Transmembrane protein 63C	4.21E-03	1.37	3.14E-02	−1.16
NAT11	N-acetyltransferase 11	1.59E-03	1.36	7.99E-03	−1.19
PLXND1	Plexin D1	2.43E-02	1.36	4.15E-02	−1.29
ATP1B1	ATPase, Na^+/K^+ transporting, beta 1 polypeptide	2.76E-02	1.36	2.58E-02	−1.37
IGFBP5	Insulin-like growth factor binding protein 5	2.44E-02	1.36	2.86E-02	−1.33
ITGB5	Integrin, beta 5	1.45E-03	1.33	7.93E-04	−1.42
EPS15	Epidermal growth factor receptor pathway substrate 15	1.01E-02	1.31	5.12E-03	−1.41
MAST4	Microtubule-associated serine/threonine kinase family member 4	1.37E-02	1.30	1.34E-02	−1.30
CAMK2N1	Calcium/calmodulin-dependent protein kinase II inhibitor 1	4.60E-02	1.29	3.41E-02	−1.34
HSP90AB1	Heat shock protein 90 kDa alpha (cytosolic), class B member 1	3.57E-02	1.29	3.94E-02	−1.27
SOAT1	Sterol O-acyltransferase (acyl-coenzyme A: cholesterol acyltransferase) 1	3.36E-03	1.28	2.65E-02	−1.12
ENAH	Enabled homolog (*Drosophila*)	8.93E-03	1.27	2.06E-03	−1.49
MIF	Macrophage migration inhibitory factor (glycosylation-inhibiting factor)	8.68E-03	1.27	1.94E-02	−1.20
KBTBD10	Kelch repeat and BTB (POZ) domain-containing 10	1.44E-03	1.26	3.46E-03	−1.19
RHOB	Ras homolog gene family, member B	2.37E-02	1.26	1.49E-03	−1.84
RNF145	Ring finger protein 145	7.85E-03	1.25	4.94E-02	−1.12
CAND1	Cullin-associated and neddylation-dissociated 1	1.30E-02	1.24	4.44E-02	−1.14
TUBB2C	Tubulin, beta 2C	3.16E-03	1.24	3.51E-03	−1.23
SQSTM1	Sequestosome 1	3.63E-02	1.23	6.86E-03	−1.46
HSPB8	Heat shock 22 kDa protein 8	1.78E-02	1.23	8.29E-03	−1.31
RBPMS2	RNA-binding protein with multiple splicing 2	1.91E-02	1.23	3.94E-02	−1.17

Continued

Table 1. Continued

Gene Symbol	Gene Name	*P* Value	Fold Change	*P* Value	Fold Change
ATF6	Activating transcription factor 6	3.49E-02	1.22	3.94E-02	−1.21
NOL8	Nucleolar protein 8	4.74E-05	1.21	6.60E-03	−1.04
SAMD9L	Sterile alpha motif domain-containing 9-like	3.83E-03	1.20	7.88E-04	−1.38
PPP1R12A	Protein phosphatase 1, regulatory (inhibitor) subunit 12A	2.00E-02	1.20	6.90E-03	−1.31
ITGB1	Integrin, beta 1 (fibronectin receptor, beta polypeptide, antigen CD29 includes MDF2, MSK12)	4.56E-02	1.20	4.37E-03	−1.53
SLC11A2	Solute carrier family 11 (proton-coupled divalent metal ion transporters), member 2	3.83E-02	1.20	4.15E-02	−1.19
PPM1E	Protein phosphatase 1E (PP2C domain containing)	1.64E-02	1.20	3.72E-02	−1.14
DYNC1LI2	Dynein, cytoplasmic 1, light intermediate chain 2	3.11E-02	1.20	1.42E-02	−1.27
ITPR1	Inositol 1,4,5-triphosphate receptor, type 1	2.56E-02	1.19	2.21E-02	−1.21
NDOR1	NADPH-dependent diflavin oxidoreductase 1	1.17E-02	1.19	3.33E-03	−1.32
DST	Dystonin	3.82E-02	1.19	1.78E-02	−1.25
CDC16	Cell division cycle 16 homolog (*Saccharomyces cerevisiae*)	3.91E-02	1.18	1.04E-02	−1.32
WDR36	WD repeat domain 36	1.04E-02	1.18	3.08E-02	−1.12
ARHGEF10	Rho guanine nucleotide exchange factor (GEF) 10	2.02E-02	1.18	4.15E-02	−1.13
LRRC51	Leucine-rich repeat containing 51	1.06E-02	1.17	4.27E-02	−1.10
PABPC4	Poly(A)-binding protein, cytoplasmic 4 (inducible form)	5.98E-03	1.17	1.08E-02	−1.14
DNAJC18	DnaJ (Hsp40) homolog, subfamily C, member 18	3.05E-02	1.17	2.13E-02	−1.20
MFGE8	Milk fat globule-EGF factor 8 protein	1.95E-02	1.17	4.36E-02	−1.12
IRF6	Interferon-regulatory factor 6	3.01E-02	1.15	1.47E-02	−1.20
ARL5A	ADP-ribosylation factor-like 5A	1.07E-04	1.15	2.01E-03	−1.05
LUZP1	Leucine zipper protein 1	3.85E-02	1.15	1.42E-02	−1.22
RAB11A	RAB11A, member RAS oncogene family	2.33E-02	1.14	7.66E-03	−1.21
THOC2	THO complex 2	8.06E-03	1.13	1.12E-02	−1.12
FBXW2	F-box and WD repeat domain-containing 2	2.22E-02	1.13	6.08E-03	−1.21
ASAH2	N-acylsphingosine amidohydrolase (nonlysosomal ceramidase) 2	4.35E-03	1.12	1.42E-02	−1.08
MYCBP	C-myc-binding protein	1.25E-02	1.12	5.37E-03	−1.16
AGPS	Alkylglycerone phosphate synthase	4.74E-02	1.11	2.64E-02	−1.14
RCC1	Regulator of chromosome condensation 1	4.75E-02	1.10	2.32E-02	−1.14
ZNF202	Zinc finger protein 202	1.72E-02	1.10	7.47E-03	−1.14
HEXA	Hexosaminidase A (alpha polypeptide)	8.52E-03	1.10	1.03E-02	−1.09
SKIV2L2	Superkiller viralicidic activity 2-like 2 (*S. cerevisiae*)	1.39E-02	1.09	2.86E-02	−1.07
DYSF	Dysferlin, limb girdle muscular dystrophy 2B (autosomal recessive)	1.66E-02	1.09	2.67E-02	−1.07
MSN	Moesin	2.68E-02	1.07	3.24E-02	−1.06
GALT	Galactose-1-phosphate uridylyltransferase	4.03E-02	1.05	3.10E-03	−1.14
ARL6	ADP-ribosylation factor-like 6	4.90E-03	1.05	8.02E-03	−1.04
Down and up		LC-TRAF2 vs WT	LC-TRAF2 vs WT	DN-TRAF2 vs WT	DN-TRAF2 vs WT
EFNB3	Ephrin B3	3.69E-05	−2.27	3.81E-03	1.19
ABHD1	Abhydrolase domain-containing 1	3.31E-04	−2.03	4.88E-03	1.33

Continued

Table 1. Continued

Gene Symbol	Gene Name	*P* Value	Fold Change	*P* Value	Fold Change
MDH1	Malate dehydrogenase 1, NAD (soluble)	8.96E-03	−1.82	2.88E-02	1.48
MAOB	Monoamine oxidase B	1.21E-04	−1.72	1.68E-02	1.11
GSTK1	Glutathione *S*-transferase kappa 1	4.46E-04	−1.71	3.02E-02	1.13
DNASE2A	Deoxyribonuclease II alpha	5.52E-05	−1.66	2.27E-02	1.07
RHD	Rh blood group, D antigen	4.76E-04	−1.50	4.62E-04	1.50
KDM5D	Lysine (K)-specific demethylase 5D	2.79E-04	−1.43	6.58E-03	1.13
ATP5E	ATP synthase, H^+ transporting, mitochondrial F1 complex, epsilon subunit	5.91E-03	−1.40	1.55E-02	1.27
LGALS4	Lectin, galactose binding, soluble 4	1.12E-03	−1.38	9.53E-03	1.17
NDUFB10	NADH dehydrogenase (ubiquinone) 1 beta subcomplex, 10	4.33E-02	−1.38	2.27E-02	1.51
DBT	Dihydrolipoamide branched chain transacylase E2	4.12E-03	−1.34	3.35E-02	1.15
C8B	Complement component 8, beta subunit	2.21E-02	−1.34	9.23E-03	1.49
CD80	CD80 antigen	5.90E-03	−1.34	1.13E-02	1.26
ATP5F1	ATP synthase, H^+ transporting, mitochondrial F0 complex, subunit b, isoform 1	2.32E-03	−1.33	5.28E-03	1.24
CHKB	Choline kinase beta	1.81E-03	−1.32	2.29E-02	1.12
FIGF	C-fos-induced growth factor	2.03E-03	−1.31	2.38E-02	1.12
APPL2	Adaptor protein, phosphotyrosine interaction, PH domain and leucine zipper-containing 2	2.16E-03	−1.31	8.06E-03	1.19
KCNH2	Potassium voltage-gated channel, subfamily H (eag-related), member 2	7.73E-03	−1.29	6.20E-03	1.32
MRPL30	Mitochondrial ribosomal protein L30	1.70E-02	−1.29	2.23E-02	1.26
SEMA5B	Sema domain, 7 thrombospondin repeats (type 1 and type 1-like), transmembrane domain (TM) and short cytoplasmic domain, (semaphorin) 5B	2.48E-03	−1.29	4.89E-03	1.22
ASB11	Ankyrin repeat and SOCS box-containing protein 11	1.27E-03	−1.29	4.41E-02	1.07
GMNN	Geminin	6.20E-03	−1.28	1.92E-02	1.18
MRPS28	Mitochondrial ribosomal protein S28	2.15E-02	−1.27	2.86E-02	1.24
GOLGA2	Golgi autoantigen, golgin subfamily a, 2	8.62E-03	−1.25	1.80E-03	1.47
DCAKD	Dephospho-CoA kinase domain containing	3.50E-02	−1.25	3.58E-02	1.24
SYNC	Syncoilin	2.32E-02	−1.25	4.54E-02	1.18
PXMP2	Peroxisomal membrane protein 2	1.37E-04	−1.24	9.15E-03	1.27
PLCXD3	Phosphatidylinositol-specific phospholipase C, X domain containing 3	5.06E-03	−1.24	1.39E-02	1.16
CCNG1	Cyclin G1	7.62E-04	−1.24	1.25E-04	1.49
NDUFB2	NADH dehydrogenase (ubiquinone) 1 beta subcomplex, 2	3.48E-02	−1.24	3.27E-02	1.24
TCEA3	Transcription elongation factor A (SII), 3	2.42E-02	−1.23	3.58E-02	1.20
MRPL47	Mitochondrial ribosomal protein L47	1.35E-02	−1.23	1.42E-03	1.58
PDYN	Prodynorphin	1.63E-03	−1.23	5.16E-03	1.15
ACADL	Acyl-coenzyme A dehydrogenase, long-chain	2.62E-02	−1.23	2.62E-03	1.60
OLFR29-PS1	Olfactory receptor 29, pseudogene 1	8.34E-03	−1.23	2.52E-02	1.15
ICT1	Immature colon carcinoma transcript 1	7.11E-03	−1.22	1.48E-02	1.17
CSDA	Cold shock domain protein A	2.78E-04	−1.22	5.70E-04	1.17

Continued

Table 1. Continued

Gene Symbol	Gene Name	*P* Value	Fold Change	*P* Value	Fold Change
CISH	Cytokine-inducible SH2-containing protein	1.73E-02	−1.22	6.49E-03	1.33
NDUFA6	NADH dehydrogenase (ubiquinone) 1 alpha subcomplex, 6 (B14)	4.11E-02	−1.21	6.94E-03	1.44
PLCB2	Phospholipase C, beta 2	4.18E-05	−1.21	1.93E-02	1.02
XLR3A	X-linked lymphocyte-regulated 3A	1.13E-02	−1.20	2.55E-02	1.15
KCNB1	Potassium voltage-gated channel, Shab-related subfamily, member 1	8.84E-03	−1.20	9.40E-03	1.20
ACIN1	Apoptotic chromatin condensation inducer 1	2.55E-02	−1.19	6.94E-03	1.32
NDUFS6	NADH dehydrogenase (ubiquinone) Fe-S protein 6	2.42E-03	−1.18	2.00E-02	1.08
UBE2G1	Ubiquitin-conjugating enzyme E2G 1 (UBC7 homolog, C. elegans)	4.22E-02	−1.18	3.65E-02	1.19
IL20RA	Interleukin-20 receptor, alpha	2.84E-02	−1.18	4.50E-02	1.15
FXC1	Fractured callus expressed transcript 1	2.15E-03	−1.17	8.43E-03	1.11
DLD	Dihydrolipoamide dehydrogenase	2.97E-02	−1.17	4.52E-03	1.35
NDUFB5	NADH dehydrogenase (ubiquinone) 1 beta subcomplex, 5	4.94E-03	−1.16	2.00E-02	1.10
TRPT1	TRNA phosphotransferase 1	4.20E-02	−1.16	1.88E-02	1.22
OLFR1352	Olfactory receptor 1352	7.35E-03	−1.15	3.58E-02	1.08
FERT2	Fer (fms/fps-related) protein kinase, testis specific 2	1.71E-03	−1.15	4.94E-03	1.10
C6	Complement component 6	6.16E-03	−1.14	2.65E-02	1.08
DUS1L	Dihydrouridine synthase 1-like (*S cerevisiae*)	9.65E-03	−1.14	3.56E-03	1.20
OLFR1335	Olfactory receptor 1335	1.21E-03	−1.13	4.37E-02	1.04
TMEM126B	Transmembrane protein 126B	4.24E-02	−1.13	2.20E-03	1.44
MRPS21	Mitochondrial ribosomal protein S21	2.64E-02	−1.13	3.65E-02	1.11
CNP	2′,3′-cyclic nucleotide 3′ phosphodiesterase	4.53E-02	−1.12	5.52E-03	1.28
UBR4	Ubiquitin protein ligase E3 component n-recognin 4	4.91E-02	−1.12	1.87E-02	1.18
CDC26	Cell division cycle 26	1.17E-02	−1.12	8.80E-03	1.13
PARP2	Poly (ADP-ribose) polymerase family, member 2	3.56E-02	−1.11	6.40E-03	1.22
COQ10A	Coenzyme Q10 homolog A (yeast)	1.71E-02	−1.11	1.43E-03	1.28
ZFP655	Zinc finger protein 655	3.09E-02	−1.11	2.50E-02	1.12
RNF113A2	Ring finger protein 113A2	1.09E-02	−1.11	3.44E-03	1.16
SPINLW1	Serine protease inhibitor-like, with Kunitz and WAP domains 1 (eppin)	2.07E-02	−1.10	1.96E-03	1.25
SULT3A1	Sulfotransferase family 3A, member 1	1.99E-03	−1.10	4.19E-02	1.03
RNASEH2A	Ribonuclease H2, large subunit	4.89E-02	−1.10	4.22E-02	1.11
RBM33	RNA-binding motif protein 33	4.26E-02	−1.10	7.29E-03	1.20
IKBKAP	Inhibitor of kappa light polypeptide enhancer in B cells, kinase complex-associated protein	4.41E-02	−1.09	1.29E-02	1.15
TRAF4	TNF receptor-associated factor 4	1.17E-02	−1.09	4.31E-03	1.13
PPP2R2D	Protein phosphatase 2, regulatory subunit B, delta isoform	4.29E-02	−1.09	1.08E-02	1.16
MRGPRB4	MAS-related GPR, member B4	3.12E-03	−1.08	3.01E-03	1.08
DPP6	Dipeptidylpeptidase 6	1.90E-02	−1.08	4.64E-03	1.14

Continued

Table 1. Continued

Gene Symbol	Gene Name	*P* Value	Fold Change	*P* Value	Fold Change
MRPL1	Mitochondrial ribosomal protein L1	1.41E-02	−1.07	3.37E-04	1.30
ARSA	Arylsulfatase A	4.48E-02	−1.07	2.77E-02	1.09
LEF1	Lymphoid enhancer-binding factor 1	2.25E-02	−1.06	1.34E-02	1.07
JMJD2C	Jumonji domain-containing 2C	1.03E-02	−1.05	2.08E-02	1.04
PCNA	Proliferating cell nuclear antigen	3.57E-02	−1.05	7.19E-04	1.23

LM indicates littermate; WT, wild type.

Table 2. Changes in Gene Expression Identified in Gene Ontology of Cellular Components

Symbol	Gene Name	Fold Change LC-TRAF2 Versus WT	Fold Change DN-TRAF2 Versus WT
Plasma membrane: up/down			
VASP	Vasodilator-stimulated phosphoprotein	1.50	−1.24
PPP1R9B	Protein phosphatase 1, regulatory (inhibitor) subunit 9B	1.37	−1.16
PLXND1	Plexin D1	1.36	−1.29
ATP1B1	ATPase, Na^+/K^+ transporting, beta 1 polypeptide	1.36	−1.37
ITGB5	Integrin, beta 5	1.33	−1.42
EPS15	Epidermal growth factor receptor pathway substrate 15	1.31	−1.41
CAMK2N1	Calcium/calmodulin-dependent protein kinase II inhibitor 1	1.29	−1.34
ENAH	Enabled homolog (*Drosophila*)	1.27	−1.49
RHOB	Ras homolog gene family, member B	1.26	−1.84
ATF6B	Activating transcription factor 6 beta	1.22	−1.21
ITGB1	Integrin, beta 1 (fibronectin receptor, beta polypeptide, antigen CD29 includes MDF2, MSK12)	1.20	−1.53
SLC11A2	Solute carrier family 11 (proton-coupled divalent metal ion transporters), member 2	1.20	−1.19
DST	Dystonin	1.19	−1.25
MFGE8	Milk fat globule-EGF factor 8 protein	1.17	−1.12
RAB11A	RAB11A, member RAS oncogene family	1.14	−1.21
ASAH2	N-acylsphingosine amidohydrolase (nonlysosomal ceramidase) 2	1.12	−1.08
DYSF	**Dysferlin, limb girdle muscular dystrophy 2B (autosomal recessive)**	1.09	−1.07
MSN	Moesin	1.07	−1.06
Plasma membrane: down/up			
MAOB	Monoamine oxidase B	−1.72	1.11
C8B	Complement component 8, beta polypeptide	−1.34	1.49
CD80	CD80 molecule	−1.34	1.26
KCNH2	Potassium voltage-gated channel, subfamily H (eag-related), member 2	−1.29	1.32
SYNC	Syncoilin, intermediate filament protein	−1.25	1.18
CSDA	Cold shock domain protein A	−1.22	1.17
CISH	Cytokine-inducible SH2-containing protein	−1.22	1.33
KCNB1	Potassium voltage-gated channel, Shab-related subfamily, member 1	−1.20	1.20
ARSA	Arylsulfatase A	−1.07	1.09

Bold indicates candidate gene selected for study.
TRAF2 indicates tumor necrosis factor receptor-associated factor 2; WT, wild type.

Table 3. Expanded Gene Lists in the Plasma Membrane Compartment

Symbol	Gene Name	Function	GO Biological Process
Plasma membrane: up/down			
VASP	Vasodilator-stimulated phosphoprotein	Ena/VASP proteins are actin-associated proteins involved in a range of processes dependent on cytoskeleton remodeling and cell polarity, such as axon guidance, lamellipodial and filopodial dynamics, platelet activation, and cell migration. VASP promotes actin filament elongation. It protects the barbed end of growing actin filaments against capping and increases the rate of actin polymerization in the presence of capping protein. VASP stimulates actin filament elongation by promoting the transfer of profilin-bound actin monomers onto the barbed end of growing actin filaments; plays a role in actin-based mobility of *Listeria* monocytogenes in host cells; regulates actin dynamics in platelets; and plays an important role in regulating platelet aggregation.	Actin polymerization or depolymerization (GO:0008154]; Neural tube closure (GO:0001843); Protein homotetramerization (GO:0051289)
PPP1R9B	Protein phosphatase 1, regulatory (inhibitor) subunit 9B	Acts as a scaffold protein in multiple signaling pathways; modulates excitatory synaptic transmission and dendritic spine morphology; binds to actin filaments (F-actin) and shows cross-linking activity; binds along the sides of the F-actin; may play an important role in linking the actin cytoskeleton to the plasma membrane at the synaptic junction; believed to target protein phosphatase 1/PP1 to dendritic spines, which are rich in F-actin, and regulates its specificity toward ion channels and other substrates, such as AMPA- and NMDA-type glutamate receptors; plays a role in regulation of G-protein-coupled receptor signaling, including dopamine D2 receptors and alpha-adrenergic receptors; binds to ADRA1B and RGS2 and mediates regulation of ADRA1B signaling; may confer to Rac signaling specificity by binding to both RacGEFs and Rac effector proteins; probably regulates p70 S6 kinase activity by forming a complex with TIAM1 (by similarity)	Cell cycle arrest (GO:0007050); cell differentiation (GO:0030154); cell migration (GO:0016477); cellular response to morphine [GO:0071315]; filopodium assembly (GO:0046847); negative regulation of cell growth (GO:0030308); nervous system development (GO:0007399); regulation of cell proliferation (GO:0042127); regulation of exit from mitosis (GO:0007096); regulation of opioid receptor-signaling pathway (GO:2000474); RNA splicing (GO:0008380)
PLXND1	Plexin D1	Cell surface receptor for SEMA4A and for class 3 semaphorins, such as SEMA3A, SEMA3C, and SEMA3E; plays an important role in cell-cell signaling, and in regulating the migration of a wide spectrum of cell types; regulates the migration of thymocytes in the medulla; regulates endothelial cell migration; plays an important role in ensuring the specificity of synapse formation; required for normal development of the heart and vasculature (by similarity); mediates antiangiogenic signaling in response to SEMA3E	Angiogenesis (GO:0001525); dichotomous subdivision of terminal units involved in salivary gland branching (GO:0060666); endothelial cell migration (GO:0043542); patterning of blood vessels (GO:0001569); regulation of angiogenesis (GO:0045765); regulation of cell migration (GO:0030334); semaphorin-plexin signaling pathway (GO:0071526); synapse assembly (GO:0007416)
ATP1B1	Sodium/potassium-transporting ATPase subunit beta-1	This is the noncatalytic component of the active enzyme, which catalyzes the hydrolysis of ATP coupled with the exchange of Na(+) and K(+) ions across the plasma membrane. The beta subunit regulates, through assembly of alpha/beta heterodimers, the number of sodium pumps transported to the plasma membrane.	ATP biosynthetic process (GO:0006754); response to hypoxia (GO:0001666); transport (GO:0006810)
ITGB5	Integrin beta-5	Integrin alpha-V/beta-5 is a receptor for fibronectin. It recognizes the sequence R-G-D in its ligand.	Cell-matrix adhesion (GO:0007160); integrin-mediated signaling pathway

Continued

Table 3. Continued

Symbol	Gene Name	Function	GO Biological Process
			(GO:0007229); multicellular organismal development (GO:0007275)
EPS15	Epidermal growth factor receptor pathway substrate 15	Involved in cell growth regulation; may be involved in the regulation of mitogenic signals and control of cell proliferation; involved in the internalization of ligand-inducible receptors of the receptor tyrosine kinase (RTK) type, in particular, EGFR; plays a role in the assembly of clathrin-coated pits (by similarity)	Cell proliferation (GO:0008283); clathrin coat assembly (GO:0048268); endocytic recycling (GO:0032456); protein transport (GO:0015031)
CAMK2N1	Calcium/calmodulin-dependent protein kinase II inhibitor 1	Potent and specific inhibitor of CaM-kinase II (CAMK2)	None listed
ENAH	Enabled homolog	Ena/VASP proteins are actin-associated proteins involved in a range of processes dependent on cytoskeleton remodeling and cell polarity, such as axon guidance and lamellipodial and filopodial dynamics in migrating cells.	Actin binding (GO:0003779); SH3 domain binding (GO:0017124); WW domain binding (GO:0050699)
RHOB	Rho-related GTP-binding protein RhoB	Mediates apoptosis in neoplastically transformed cells after DNA damage; not essential for development, but affects cell adhesion and growth factor signaling in transformed cells; plays a negative role in tumorigenesis because deletion causes tumor formation; involved in intracellular protein trafficking of a number of proteins; targets PKN1 to endosomes and is involved in trafficking of the EGF receptor from late endosomes to lysosomes; also required for stability and nuclear trafficking of AKT1/AKT, which promotes endothelial cell survival during vascular development; serves as a microtubule-dependent signal that is required for the myosin contractile ring formation during cell cycle cytokinesis; required for genotoxic stress-induced cell death in breast cancer cells.	Angiogenesis (GO:0001525); apoptotic process (GO:0006915); cell adhesion (GO:0007155); cell cycle cytokinesis (GO:0033205); cellular response to hydrogen peroxide (GO:0070301); Cellular response to ionizing radiation (GO:0071479); endosome to lysosome transport (GO:0008333); GTP catabolic process (GO:0006184); negative regulation of cell cycle (GO:0045786); positive regulation of angiogenesis (GO:0045766); positive regulation of apoptotic process (GO:0043065); protein transport (GO:0015031); Rho protein signal transduction (GO:0007266); transformed cell apoptotic process (GO:0006927)
ATF6B	Activating transcription factor 6 beta	Transcriptional factor that acts in the unfolded protein response (UPR) pathway by activating UPR target genes induced during ER stress; binds DNA on the 5′-CCAC[GA]-3′ half of the ER stress response element (ERSE) (5′-CCAATN(9)CCAC[GA]-3′) when NF-Y is bound to ERSE	Regulation of transcription, DNA dependent (r0:0006355); response to unfolded protein (GO:0006986); signal transduction (GO:0007165); transcription, DNA dependent (GO:0006351)
ITGB1	Integrin beta-1	Integrins alpha-1/beta-1, alpha-2/beta-1, alpha-10/beta-1, and alpha-11/beta-1 are receptors for collagen. Integrins alpha-1/beta-1 and alpha-2/beta-2 recognize the proline-hydroxylated sequence G-F-P-G-E-R in collagen. Integrins alpha-2/beta-1, alpha-3/beta-1, alpha-4/beta-1, alpha-5/beta-1, alpha-8/beta-1, alpha-10/beta-1, alpha-11/beta-1, and alpha-V/beta-1 are receptors for fibronectin. Integrin alpha-1/beta-1, alpha-2/beta-1, alpha-6/beta-1, and alpha-7/beta-1 are receptors for lamimin. Integrin alpha-9/beta-1 is a receptor for VCAM1, cytotactin, and osteopontin. It recognizes the sequence A-E-I-D-G-I-E-L in cytotactin. Integrin alpha-3/beta-1 is a receptor for epiligrin, thrombospondin, and CSPG4. Integrin alpha-V/beta-1 is a receptor for vitronectin.	B cell differentiation (GO:0030183); calcium-independent cell-matrix adhesion (GO:0007161); cardiac muscle cell differentiation (GO:0055007); cell fate specification (GO:0001708); cell migration (GO:0016477); cell migration involved in sprouting angiogenesis (GO:0002042); cell-cell adhesion mediated by integrin (GO:0033631); cell-matrix adhesion (GO:0007160); cellular defense response (GO:0006968); cellular response to ionizing radiation (GO:0071479); cellular response to vitamin D (GO:0071305); G_1/S transition of mitotic cell cycle (GO:0000082); germ cell migration (GO:0008354); homophilic cell adhesion (GO:0007156); in utero

Continued

Table 3. Continued

Symbol	Gene Name	Function	GO Biological Process
			embryonic development (GO:0001701); integrin-mediated signaling pathway (GO:0007229); interspecies interaction between organisms (GO:0044419); leukocyte cell-cell adhesion (GO:0007159); maternal process involved in female pregnancy (GO:0060135); negative regulation of cell projection organization (GO:0031345); negative regulation of cell proliferation (GO:0008285); negative regulation of neuron differentiation (GO:0045665); positive regulation of apoptotic process (GO:0043065); positive regulation of cell migration (GO:0030335); any process that activates or increases the frequency, rate, or extent of cell migration; positive regulation of cell proliferation (GO:0008284); positive regulation of cell-substrate adhesion (GO:0010811); positive regulation of endocytosis (GO:0045807); positive regulation of MAPK cascade (GO:0043410); positive regulation of neuron differentiation (GO:0045666); positive regulation of neuron projection development (GO:0010976); positive regulation of peptidyl-tyrosine phosphorylation (GO:0050731); protein transport within lipid bilayer (GO:0032594); regulation of cell cycle (GO:0051726); regulation of G-protein-coupled receptor protein signaling pathway (GO:0008277); response to activity (GO:0014823); response to drug (GO:0042493); response to gonadotropin stimulus (GO:0034698); response to transforming growth factor beta stimulus (GO:0071559); sarcomere organization (GO:0045214); tight junction assembly (GO:0070830); tissue homeostasis (GO:0001894)
SLC11A2	Solute carrier family 11 (proton-coupled divalent metal ion transporters), member 2	Important in metal transport, in particular, iron; can also transport manganese, cobalt, cadmium, nickel, vanadium, and lead; involved in apical iron uptake into duodenal enterocytes; involved in iron transport from acidified endosomes into the cytoplasm of erythroid precursor cells; may play an important role in hepatic iron accumulation and tissue iron distribution	Activation of cysteine-type endopeptidase activity involved in apoptotic process (GO:0006919); cellular response to oxidative stress (GO:0034599); transport of cobalt, cadmium, copper, iron, lead, nickel, vanadium, and zinc (GO:multiple terms); hydrogen ion transmembrane transporter activity; dendrite morphogenesis (GO:0048813); learning or memory (GO:0007611)
DST	Dystonin	Cytoskeletal linker protein; acts as an integrator of intermediate filaments, actin, and microtubule cytoskeleton networks; required for anchoring either intermediate filaments to the actin cytoskeleton in neural and muscle cells or keratin-containing intermediate filaments to hemidesmosomes in	Axonogenesis (GO:0007409); cell adhesion (GO:0007155); cell cycle arrest (GO:0007050); cell motility (GO:0048870); cytoplasmic microtubule organization (GO:0031122); cytoskeleton organization (GO:0007010); hemidesmosome assembly

Continued

Table 3. Continued

Symbol	Gene Name	Function	GO Biological Process
		epithelial cells; the proteins may self-aggregate to form filaments or a two-dimensional mesh.	(GO:0031581); integrin-mediated signaling pathway (GO:0007229); intermediate filament cytoskeleton organization (GO:0045104); maintenance of cell polarity (GO:0030011); microtubule cytoskeleton organization (GO:0000226); regulation of microtubule polymerization or depolymerization (GO:0031110); response to wounding (GO:0009611); retrograde axon cargo transport (GO:0008090)
MFGE8	Lactadherin	Plays an important role in the maintenance of intestinal epithelial homeostasis and the promotion of mucosal healing; promotes VEGF-dependent neovascularization (by similarity); contributes to phagocytic removal of apoptotic cells in many tissues; specific ligand for the alpha-v/beta-3 and alpha-v/beta-5 receptors; also binds to phosphatidylserine-enriched cell surfaces in a receptor-independent manner; zona pellucida-binding protein, which may play a role in gamete interaction; binds specifically to rotavirus and inhibits its replication	Angiogenesis (GO:0001525); cell adhesion (GO:0007155); interspecies interaction between organisms (GO:0044419); phagocytosis, engulfment (GO:0006911); phagocytosis, recognition (GO:0006910); positive regulation of apoptotic cell clearance (GO:2000427); positive regulation of cell proliferation (GO:0008284); response to estrogen stimulus (GO:0043627); single fertilization (GO:0007338)
RAB11A	RAB11a, member RAS oncogene family	Regulates endocytic recycling; may exert its functions by interacting with multiple effector proteins in different complexes; acts as a major regulator of membrane delivery during cytokinesis; together with MYO5B and RAB8A, participates in epithelial cell polarization; together with RAB3IP, RAB8A, the exocyst complex, PARD3, PRKCI, ANXA2, CDC42, and DNMBP, promotes transcytosis of PODXL to the apical membrane initiation sites (AMIS), apical surface formation, and lumenogenesis (by similarity); together with MYO5B, participates in CFTR trafficking to the plasma membrane and TF (transferrin) recycling in nonpolarized cells; required in a complex with MYO5B and RAB11FIP2 for the transport of NPC1L1 to the plasma membrane; participates in the sorting and basolateral transport of CDH1 from the Golgi apparatus to the plasma membrane; regulates the recycling of FCGRT (receptor of Fc region of monomeric IgG) to basolateral membranes (by similarity)	Cell cycle (GO:0007049) cytokinesis (GO:0000910); GTP catabolic process (GO:0006184); neuron projection development (GO:0031175); plasma membrane to endosome transport (GO:0048227); protein localization in plasma membrane (GO:0072659); regulation of long-term neuronal synaptic plasticity (GO:0048169); regulation of protein transport (GO:0051223); small GTPase-mediated signal transduction (GO:0007264); vesicle-mediated transport (GO:0016192)
ASAH2	N-acylsphingosine amidohydrolase (nonlysosomal ceramidase) 2 (neutral sphingomyelinase)	Hydrolyzes the sphingolipid ceramide into sphingosine and free fatty acid at an optimal pH of 6.5 to 8.5; acts as a key regulator of sphingolipid signaling metabolites by generating sphingosine at the cell surface; acts as a repressor of apoptosis both by reducing C16-ceramide, thereby preventing ceramide-induced apoptosis, and generating sphingosine, a precursor of the antiapoptotic factor, sphingosine 1-phosphate; probably involved in the digestion of dietary sphingolipids in intestine by acting as a key enzyme for the catabolism of dietary sphingolipids and regulating the levels of bioactive sphingolipid metabolites in the intestinal tract	Apoptotic process (GO:0006915); ceramide metabolic process (GO:0006672); signal transduction (GO:0007165)
DYSF	Dysferlin	Key calcium ion sensor involved in the Ca(2+)-triggered synaptic key calcium ion sensor involved in Ca(2+)-	None identified

Continued

Table 3. Continued

Symbol	Gene Name	Function	GO Biological Process
		triggered synaptic vesicle-plasma membrane fusion; plays a role in the sarcolemma repair mechanism of both skeletal muscle and cardiomyocytes that permits rapid resealing of membranes disrupted by mechanical stress	
MSN	Moesin	Probably involved in connections of major cytoskeletal structures to the plasma membrane; may inhibit herpes simplex virus 1 infection at an early stage	Cellular component movement (GO:0006928); leukocyte cell-cell adhesion (GO:0007159); leukocyte migration (GO:0050900); membrane-to-membrane docking (GO:0022614); regulation of lymphocyte migration (GO:2000401)
Plasma membrane: down/up			
MAOB	Monoamine oxidase B	Catalyzes the oxidative deamination of biogenic and xenobiotic amines and has important functions in the metabolism of neuroactive and vasoactive amines in the central nervous system and peripheral tissues; MAOB preferentially degrades benzylamine and phenylethylamine.	Negative regulation of serotonin secretion (GO:0014063); positive regulation of dopamine metabolic process (GO:0045964); response to aluminum ion (GO:0010044); response to corticosterone stimulus (GO:0051412); response to drug (GO:0042493); response to ethanol (GO:0045471); response to lipopolysaccharide (GO:0032496); response to selenium ion (GO:0010269); response to toxin (GO:0009636)
C8B	Complement component 8, beta subunit	Constituent of the membrane attack complex (MAC) that plays a key role in the innate and adaptive immune response by forming pores in the plasma membrane of target cells	Complement activation (GO:0006956); complement activation, alternative pathway (GO:0006957); complement activation, classical pathway (GO:0006958); cytolysis (GO:0019835); immune response (GO:0006955)
CD80	T-lymphocyte activation antigen CD80	Involved in the costimulatory signal essential for T-lymphocyte activation; T-cell proliferation and cytokine production is induced by the binding of CD28 or CTLA-4 to this receptor.	Cell-cell signaling (GO:0007267); interspecies interaction organisms (GO:0044419); intracellular signal transduction (GO:0035556); positive regulation of alpha-beta T-cell proliferation (GO:0046641); positive regulation of the granulocyte macrophage colony-stimulating factor biosynthetic process (GO:0045425); positive regulation of the interleukin-2 biosynthetic process (GO:0045086); Positive regulation of peptidyl-tyrosine phosphorylation (GO:0050731); positive regulation of signal transduction (GO:0009967); positive regulation of T-helper 1 cell differentiation (GO:0045627); positive regulation of transcription, DNA dependent (GO:0045893); T-cell activation (GO:0042110)
KCNH2	Potassium voltage-gated channel subfamily H member 2	Pore-forming (alpha) subunit of voltage-gated inwardly rectifying potassium channel; channel properties are modulated by cAMP and subunit assembly; mediates the rapidly activating component of the delayed rectifying potassium current in heart (IKr)	Blood circulation (GO:0008015); muscle contraction (GO:0006936); potassium ion transport (GO:0006813); protein heterooligomerization (GO:0051291); regulation of heart contraction (GO:0008016); regulation of membrane

Continued

Table 3. Continued

Symbol	Gene Name	Function	GO Biological Process
			potential (GO:0042391); regulation of transcription, DNA dependent (GO:0006355)
SYNC	Syncoilin	Intermediate filament	Intermediate filament-based process (GO:0045103)
CSDA	Cold shock domain protein A	Binds to the GM-CSF promoter; seems to act as a repressor; binds also to full-length mRNA and to short RNA sequences containing the consensus site 5′-UCCAUCA-3′; may have a role in translation repression	Fertilization (GO:0009566); in utero embryonic development (GO:0001701); male gonad development (GO:0008584); negative regulation of apoptotic process (GO:0043066); negative regulation of skeletal muscle tissue development (GO:0048642); negative regulation of transcription from RNA polymerase II promoter (GO:0000122); organ regeneration (GO:0031100); positive regulation of organ growth (GO:0046622); regulation of transcription, DNA dependent (GO:0006355); response to cold (GO:0009409); spermatogenesis (GO:0007283); transcription, DNA dependent (GO:0006351); positive regulation of organ growth (GO:0046622)
CISH	Cytokine inducible SH2-containing protein	SOCS family proteins form part of a classical negative feedback system that regulates cytokine signal transduction. CIS is involved in the negative regulation of cytokines that signal through the JAK-STAT5 pathway, such as erythropoietin, prolactin, and interleukin-3 (IL-3) receptor. Inhibits STAT5 transactivation by suppressing its tyrosine phosphorylation; may be a substrate-recognition component of an SCF-like ECS (Elongin BC-CUL2/5-SOCS-box protein) E3 ubiquitin-protein ligase complex, which mediates the ubiquitination and subsequent proteasomal degradation of target proteins (by similarity).	Intracellular signal transduction (GO:0035556); negative regulation of signal transduction (GO:0009968); protein ubiquitination (GO:0016567); regulation of cell growth (GO:0001558)
KCNB1	Potassium voltage-gated channel subfamily B member 1	Mediates the voltage-dependent potassium ion permeability of excitable membranes; channels open or close in response to the voltage difference across the membrane, letting potassium ions pass in accord with their electrochemical gradient	Protein homooligomerization (GO:0051260)
ARSA	Arylsulfatase A	Hydrolyzes cerebroside sulfate	None identified

dysferlin as a potential candidate gene for the cytoprotective effects of TRAF2.

NF-κB-Induced Activation of Dysferlin Gene Expression

Previous studies from this laboratory have suggested that TNF/TRAF2-mediated activation of NF-κB is responsible for provoking cytoprotective responses in the heart after I/R injury.[11] Previously, we have reported that both RelB and p52 were upregulated in hearts of MHC-TRAF2$_{LC}$ mice, when compared to LM controls.[19] To determine whether components of noncanonical NF-κB signaling were responsible for the observed increased in dysferlin expression in MHC-TRAF2$_{LC}$ mouse hearts, we performed a ChIP assay. As shown in Figure 7, there was a significant 2-fold increase in RelB binding to the dysferlin (variant 1) promoter in MHC-TRAF2$_{LC}$ hearts, when compared to WT hearts, which was accompanied by significant binding of p50 and p52, which are potential binding partners for RelB. These experiments suggest that TRAF2-mediated activation of NF-κB contributed to increased dysferlin expression observed in MHC-TRAF2$_{LC}$ hearts.

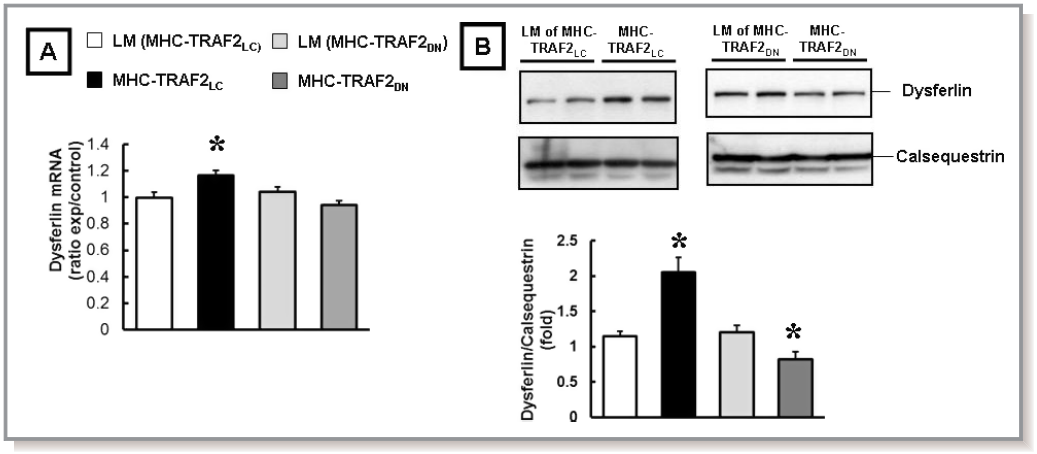

Figure 6. Expression levels of dysferlin mRNA and protein levels in MHC-TRAF2$_{LC}$, MHC-TRAF2$_{DN}$, and littermate (LM) control) mice. A, mRNA levels in naïve 12-week-old MHC-TRAF2$_{LC}$ and MHC-TRAF2$_{DN}$, relative to respective LM control hearts (n=6/group). B, Representative Western blot of dysferlin protein levels in naïve 12-week-old MHC-TRAF2$_{LC}$ and MHC-TRAF2$_{DN}$ and group data for dysferlin protein (relative to calsequestrin) in MHC-TRAF2$_{LC}$ and MHC-TRAF2$_{DN}$ hearts (n=8/group). *P<0.05, compared to the respective LM control. TRAF2 indicates tumor necrosis factor receptor-associated factor 2.

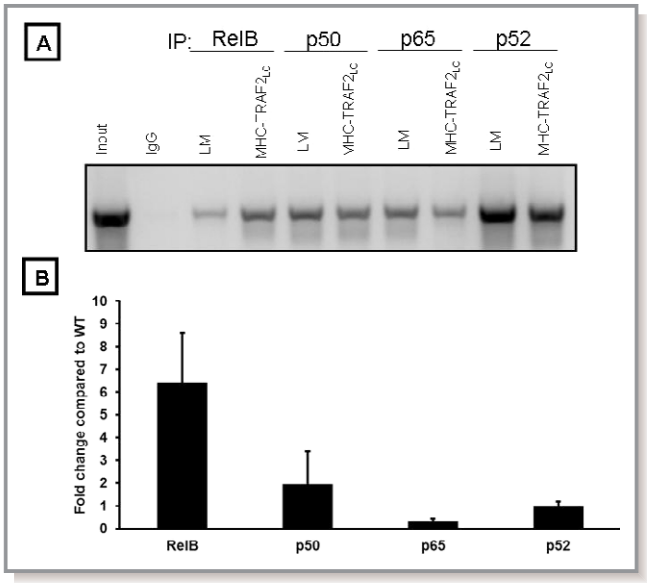

Figure 7. NF-κB chromatin immunprecipitation (ChIP). RelB, p50, p65, and p52 antibodies were used for ChIP on mouse heart chromatin. Presence of NF-κB family members at a κB site in the dysferlin promoter was detected by PCR and expressed as fold change relative to WT controls (n=3). LM indicates littermate; NF-κB, nuclear factor kappa B; PCR, polymerase chain reaction; TRAF2, tumor necrosis factor receptor-associated factor 2; WT, wild type.

Characterization of the Dysferlin-Null Mice

Phenotypic Characterization of Dysferlin-Null (Dysferlin$^{-/-}$) Mice

In order to explore the role of dysferlin as a potential mediator of the cytoprotective effects of TRAF2, we first characterized the phenotype of the dysferlin-null (dysferlin$^{-/-}$) mice employed in these studies. Figure 8A shows that 12-week-old dysferlin$^{-/-}$ mice had no obvious LV phenotype, as assessed by gross morphology and H&E staining. There was, however, a small, but significant, increase in the heart weight/body weight ratio in dysferlin$^{-/-}$ mice, when compared to WT controls (Figure 8B). 2D-targeted M-mode echo disclosed no significant differences in LV fractional shortening (Figure 8C) or LVDP (Figure 8D), LV +dP/dt (Figure 8E) and LV −dP/dt (Figure 8F), or LV dimensions (Figure 8G through 8I) between dysferlin$^{-/-}$ knockout mice, compared to WT controls.

I/R Injury

Although previous studies in dysferlin-null mice have failed to demonstrate a role for dysferlin in reducing infarct size after acute coronary ligation in vivo,[14] the role of dysferlin after I/R injury (wherein the mechanisms of cell injury are different) is not known. Accordingly, we subjected dysferlin$^{-/-}$ mouse hearts to 30 minutes of global ischemia, followed by 60 minutes of reperfusion. The salient finding shown by Figure 9A is that LV functional recovery after I/R injury was significantly (P<0.001 by ANOVA) worse in dysferlin-null hearts, when compared to WT. Differences in LVDP were evident 20 minutes after reperfusion and remained significantly worse than WT controls 60 minutes after reperfusion (P<0.05/time). Importantly, both myocardial CK release (Figure 9B) and degree of uptake of Evans blue dye (Figure 9C and 9D) were significantly increased (P<0.05 for both) in hearts of I/R-injured dysferlin-null mice, when compared to WT controls. These results are consistent with the thesis that dysferlin-mediated membrane repair is important for main-

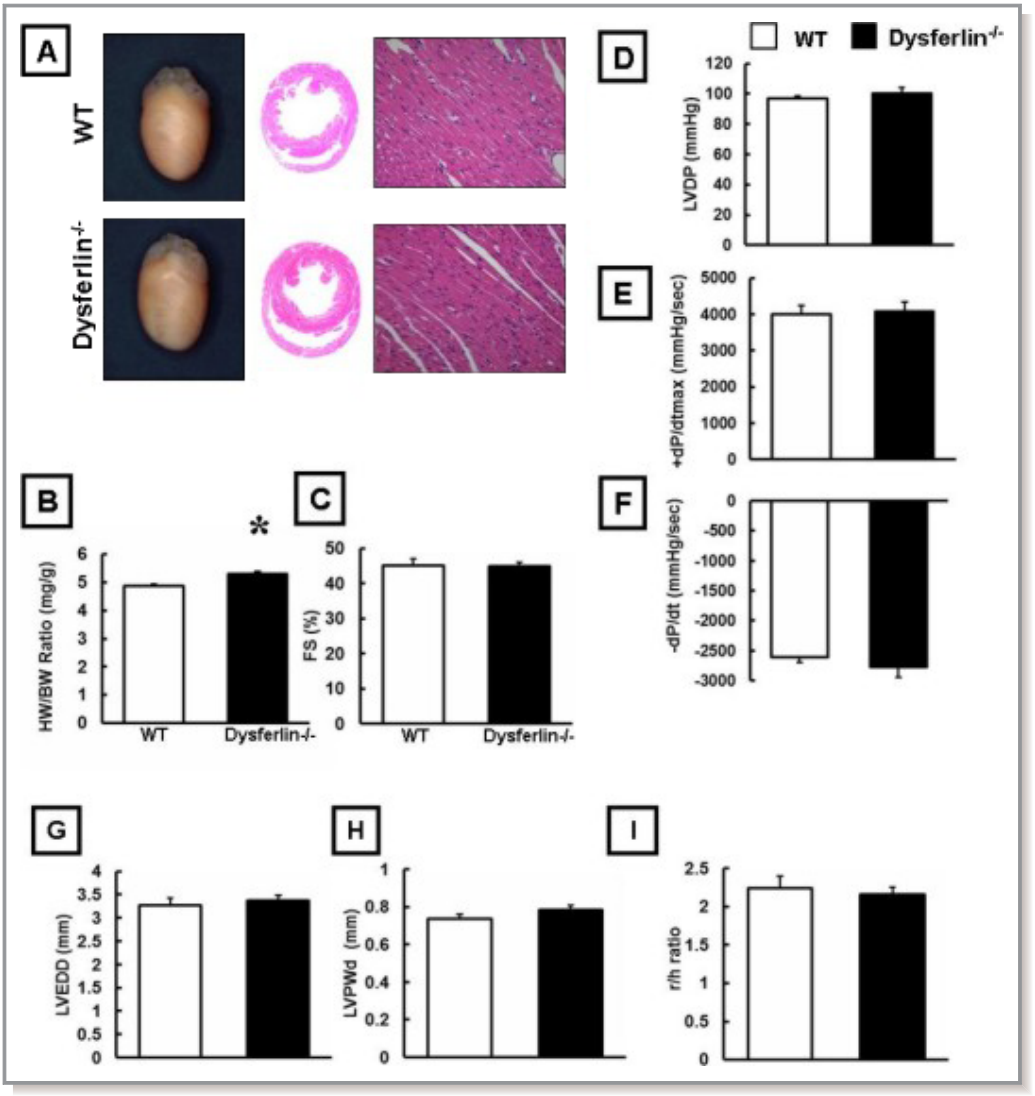

Figure 8. Characterization of dysferlin-null (dysferlin$^{-/-}$) mice. Dysferlin$^{-/-}$ and wild-type (WT) control mice were 12 weeks of age. A, Representative photographs of dysferlin$^{-/-}$ and WT control hearts; hematoxylin and eosin–stained cross-sections at the level of the papillary muscle and representative hematoxylin and eosin–stained cross sections at the level of the papillary muscles (×400). B, Heart weight/body weight ratio (n=6/group) of dysferlin$^{-/-}$ hearts and WT controls. C, Percent LV fractional shortening (% FS) in 12-week-old dysferlin$^{-/-}$ hearts (n=9) and WT controls (n=6). D, Percent LV developed pressure (% LVDP) ex vivo (n=6 hearts/group). E and F, LV +dP/d*t* and LV −dP/d*t* ex vivo (n=9/group). G, LV end-diastolic dimension (LVEDD), (H) LV posterior wall diameter (LVPWd), and (I) ratio of LV radius to LV wall thickness (r/h). **P*<0.05, compared to the respective WT control. BW indicates body weight; HW, heart weight; LV, left ventricle.

taining membrane integrity and LV functional recovery after I/R injury.

Effects of Dysferlin on TRAF2-Mediated Cytoprotection After I/R Injury

To determine whether the cytoprotective effects of TRAF2 were mediated, at least in part, through dysferlin, we generated MHC-TRAF2$_{LC}$/dysferlin$^{-/-}$ mice and subjected these hearts to I/R injury. The important finding shown by Figure 10A is that the cytoprotective effects of TRAF2 were attenuated significantly in a dysferlin-null background. As shown, functional recovery in MHC-TRAF2$_{LC}$/dysferlin$^{-/-}$ mice was significantly less than MHC-TRAF2$_{LC}$ mice at 10 to 60 minutes (*P*<0.05/time point) after reperfusion. Furthermore, there was a significant increase in myocardial CK release (Figure 10B) and degree of uptake of Evans blue dye (Figure 10C and 10D; *P*<0.05 for both) in hearts of I/R-

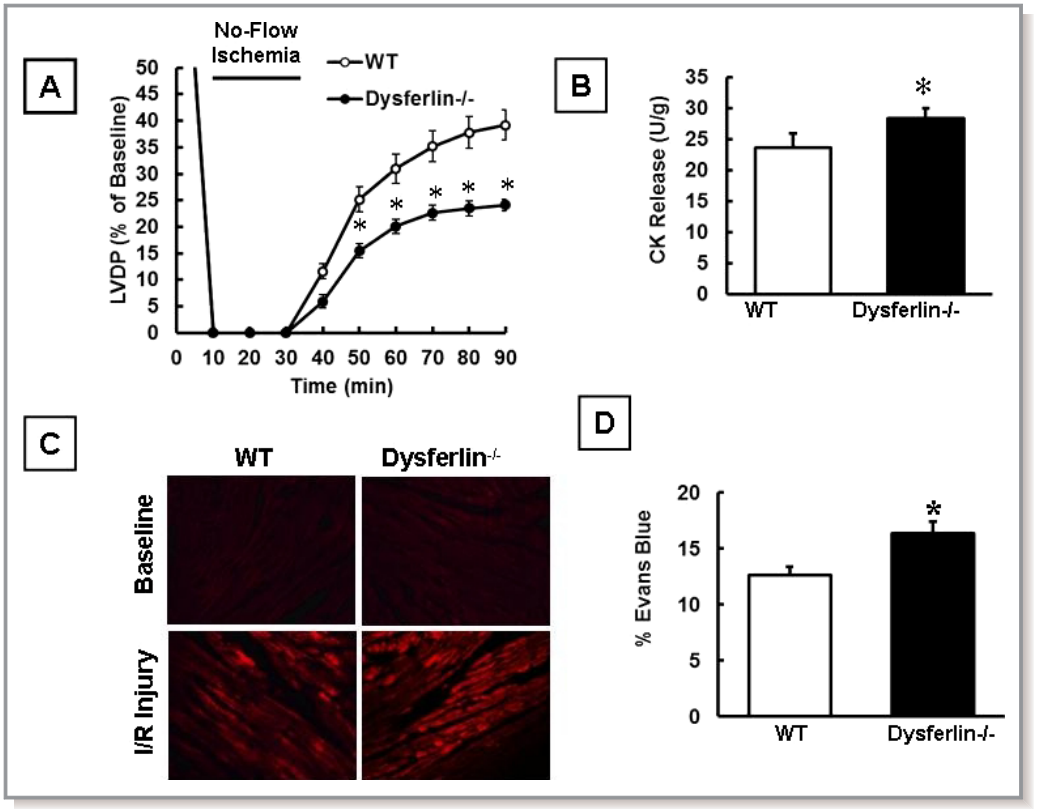

Figure 9. Effects of ischemia-reperfusion (I/R) injury in dysferlin-null (dysferlin$^{-/-}$) mice and wild-type (WT) control mice. Dysferlin$^{-/-}$ and WT control mice were 12 weeks of age. A, Percent LV developed pressure after I/R injury (n=6 hearts/group). B, Creatine kinase (CK) release in the effluent at baseline and 30 minutes after I/R injury (n=6 hearts/group). C, Representative images of Evans blue dye uptake. D, Group data for Evans blue dye uptake at baseline and 30 minutes after I/R injury (n=6 hearts/group). *P<0.05, compared to WT controls. LV indicates left ventricle; LVDP, LV developed pressure.

injured MHC-TRAF2$_{LC}$/dysferlin$^{-/-}$ mice, when compared to MHC-TRAF2$_{LC}$ mice. A second important finding shown in Figure 10A is that the overall degree of functional recovery in the MHC-TRAF2$_{LC}$/dysferlin$^{-/-}$ mice was significantly greater than WT control mice (P<0.001), suggesting that the cytoprotective effects of TRAF2 are not exclusively mediated through dysferlin.

To determine whether I/R injury resulted in differential localization of dysferlin in cardiac myocytes from MHC-TRAF$_{LC}$ mouse hearts, compared to LM controls, we performed IHC staining at baseline in naïve hearts and 60 minutes after I/R injury. As shown by the representative photomicrographs in Figure 11, dysferlin was not immunodetectable in cardiac myocytes from LM controls or MHC-TRAF$_{LC}$ mouse hearts. It contrast, after I/R injury, dysferlin was weakly detectable in the cytoplasm of scattered cardiac myocytes from control hearts, whereas dysferlin immunostaining was easily detectable at the intercalated disks and diffusely throughout the cytoplasm of cardiac myocytes from MHC-TRAF$_{LC}$ mouse hearts, suggesting that TRAF2 signaling resulted in increased dysferlin trafficking to the membrane of MHC-TRAF$_{LC}$ mouse hearts.

Discussion

The results of this study, in which we employed both gain- and loss-of-function approaches to delineate the mechanism(s) for the cytoprotective effects of TRAF2, suggest that TRAF2-mediated upregulation of dysferlin is responsible, at least in part, for the cytoprotective effects of TRAF2 after I/R injury. As shown in Figure 3A, Tg mouse lines with cardiac-restricted overexpression of low levels of TRAF2 (MHC-TRAF2$_{LC}$) had improved LV functional recovery after I/R injury, relative to LM controls, whereas mice with cardiac-restricted overexpression of MHC-TRAF2$_{DN}$ had decreased LV functional recovery after I/R injury. Decreased functional recovery in MHC-TRAF2$_{DN}$ mice was accompanied by increased CK release (Figure 3B) and Evans blue dye uptake (Figure 3C and 3D), consistent with increased membrane permeability. Improved functional recovery in MHC-TRAF2$_{LC}$ mice is associated with decreased CK release and decreased Evans blue dye uptake, consistent with enhanced membrane stability.[11] To delineate the mechanisms for the cytoprotective effects of TRAF2, we performed transcriptional profiling in

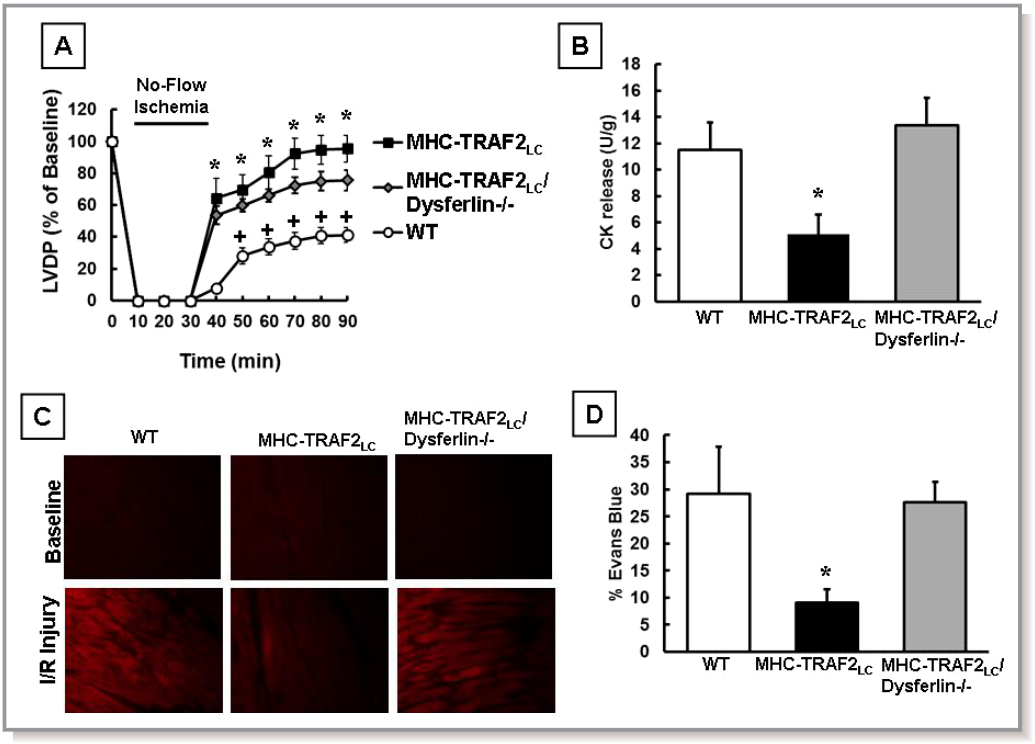

Figure 10. Effects of ischemia-reperfusion (I/R) injury in MHC-TRAF2$_{LC}$, MHC-TRAF2$_{LC}$/dysferlin$^{-/-}$, and littermate (LM) controls. All studies were performed in 12-week-old mice (see Methods for breeding strategy). A, Percent LV developed pressure after I/R injury (n=6 to 7 hearts/group). B, Creatine kinase (CK) release in the effluent at baseline and 30 minutes after I/R injury (n=6 hearts/group). C, Representative images of Evans blue dye uptake. D, Group data for Evans blue dye uptake at baseline and 30 minutes after I/R injury (n=3 control hearts; n=4 dysferlin$^{-/-}$ hearts). *P<0.05 and compared to WT controls; ^{+}P<0.05, compared to MHC-TRAF2$_{LC}$/dysferlin$^{-/-}$). LM indicates littermate; LV, left ventricle; LVDP, LV developed pressure; TRAF2, tumor necrosis factor receptor-associated factor 2; WT, wild type.

MHC-TRAF2$_{LC}$ and MHC-TRAF2$_{DN}$ mouse hearts. Using this unbiased strategy, we identified a calcium-triggered exocytotic membrane repair protein, termed dysferlin, as a potential candidate cytoprotective gene downstream from TRAF2-mediated signaling (Figure 4 and Table 2). Importantly, dysferlin mRNA and protein were significantly upregulated in MHC-TRAF2$_{LC}$ mice, whereas dysferlin protein was significantly downregulated in MHC-TRAF2$_{DN}$ mice (Figure 6). Moreover, dysferlin was immunolocalized to the intercalated disks and diffusely throughout the cytoplasm of cardiac myocytes from MHC-TRAF2$_{LC}$ mouse hearts after I/R injury, whereas it was weakly detectable in the cytoplasm of WT control hearts (Figure 11). Consistent with our earlier observations, which have implicated an important role for NF-κB signaling in terms of mediating the cytoprotective effects of the TNF-TRAF2-signaling pathway,[11] the ChIP assay identified RelB, p50, and p52 binding in the promoter region of the dysferlin gene (Figure 7). Characterization of dysferlin-null mice revealed that they had decreased functional LV recovery, increased CK release, and increased Evans blue dye uptake after I/R injury (Figure 9), thus phenocopying the response to I/R injury observed in MHC-TRAF2$_{DN}$ mice. Finally, breeding MHC-TRAF2$_{LC}$ mice onto a dysferlin-null background (MHC-TRAF2$_{LC}$/dysferlin$^{-/-}$) resulted in increased tissue injury, increased Evans Blue dye uptake, and decreased functional recovery, when compared to MHC-TRAF2$_{LC}$ mice (Figure 10), suggesting that dysferlin mediates, at least in part, the cytoprotective effects of TRAF2. Importantly, functional recovery in MHC-TRAF2$_{LC}$/dysferlin$^{-/-}$ mice after I/R injury was still significantly greater than observed in WT controls (Figure 10A), suggesting that cytoprotective effects of TRAF2 are not mediated exclusively through dysferlin. Indeed, TRAF2 mediates mitophagy through an E3 ligase-dependent mechanism in the adult heart.[21] Although speculative, these results suggest that the cytoprotective effects of TRAF2 may relate to clearance of mitochondria that are damaged after I/R injury.

Dysferlin-Mediated Membrane Repair in the Mammalian Heart

Given that maintenance of plasma membrane integrity is required for cell viability, it is not surprising that cells have

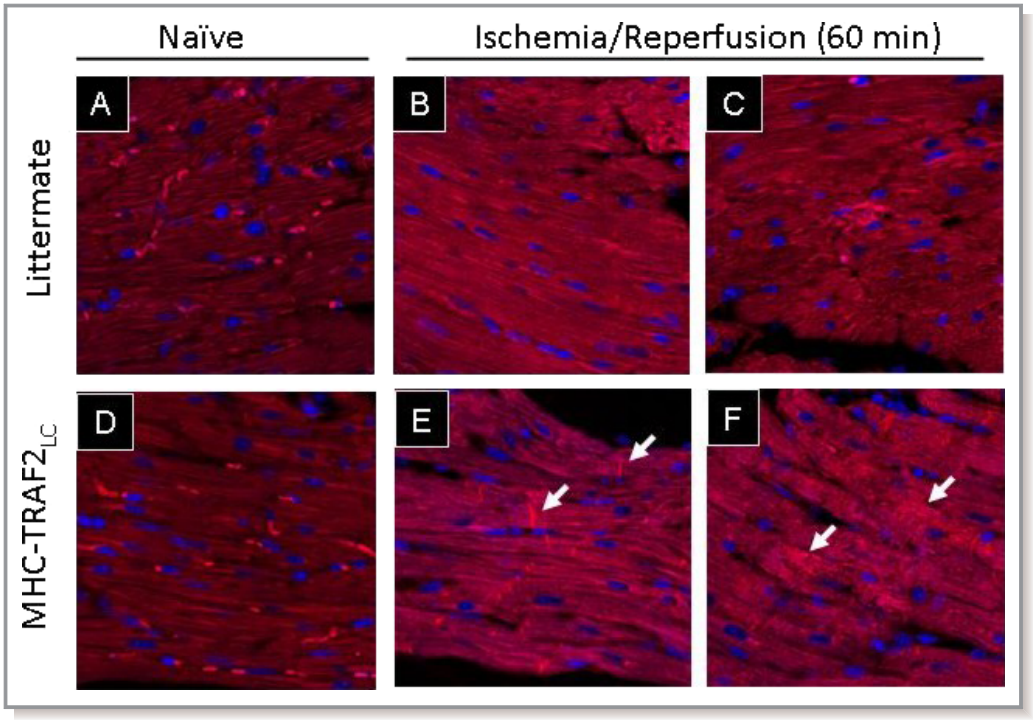

Figure 11. Dysferlin immuohistochemical staining in littermate controls and MHC-$TRAF_{LC}$ mouse hearts. In naïve hearts, dysferlin was not immunodetectable in cardiac myocytes from littermate controls (A) or MHC-$TRAF_{LC}$ mouse hearts (B). In contrast, after I/R injury, dysferlin was weakly detectable in the cytoplasm of scattered cardiac myocytes from control hearts (B and C). As shown by arrows, dysferlin immunostaining was easily detectable at the intercalated disks (E) and diffusely throughout the cytoplasm (F) of cardiac myocytes from MHC-$TRAF_{LC}$ mouse hearts, suggesting that TRAF2 signaling resulted in increased dysferlin trafficking to the membrane of the MHC-$TRAF_{LC}$ mouse heart. I/R indicates ischemia reperfusion; TRAF2, tumor necrosis factor receptor-associated factor 2.

evolved a variety of different "emergency repair" mechanisms to facilitate plasma membrane resealing under physiologic and pathophysiologic conditions. This is particularly important for cells residing in mechanically stressful environments, such as cardiac and/or skeletal myocytes.[20,22–24] In mammalian cells, plasma membranes reseal spontaneously if the lesion is small (<1 μmol/L). If the membrane lesion is large (>1 μmol/L), nucleated cells use an active membrane repair process that is based on Ca^{2+}-triggered active trafficking of cytoplasmic vesicles to the site of membrane damage with subsequent fusion of vesicles with the plasma membrane (exocytosis), thereby creating a "patch" of new membrane across the gap in the plasma membrane. The process of active membrane fusion during exocytosis requires several membrane proteins, including SNARE proteins,[25] synaptotagmins,[26] and a recently described muscle-specific TRIM protein, MG53, that is important in sarcolemmal repair in ischemic preconditioning.[27]

Recently, a family of proteins termed "ferlins" has been shown to play an important role in membrane repair by facilitating Ca^{2+}-mediated trafficking of vesicles to the site of membrane injury. The ferlin family consists of four different highly conserved genes that encode dysferlin, myoferlin, otoferlin, and Fer1L4 (reviewed previously[25]). Dysferlin is a 273 kDa type II transmembrane protein that is enriched in skeletal and cardiac muscle.[20] Mutations in dysferlin lead to three distinct muscular dystrophies ("dysferlinopathies"): limb-girdle muscular dystrophy type 2B;[28] Miyoshi myopathy;[28] and distal myopathy with anterior tibialis onset. Although onset of dilated cardiomyopathy is extremely rare in dysferlinopathies, ≈50% of patients develop mild structural (increased myocardial fibrosis) and functional (diastolic dysfunction) cardiac abnormalities.[29,30] These findings are consistent with experimental studies that have shown that aging dysferlin-deficient mice develop progressive myocardial fibrosis by 10 to 12 months of age, suggesting an important role for membrane repair mechanisms in aging hearts.[14,31]

Relevant to the present study, dysferlin deficiency has been implicated in the development of a dilated cardiomyopathic phenotype after adrenergic and/or mechanical stress.[14,30] Han et al. demonstrated increased cardiac myocyte membrane permeability (increased Evans blue dye uptake) and progressive LV dysfunction in exercising dysferlin-null mice. Although these researchers did not demonstrate a role for dysferlin in reducing

infarct size after acute coronary ligation, they did not examine the role of dysferlin in I/R injury, wherein the mechanisms of cell injury are different. Our results are in agreement with these earlier studies that have demonstrated an important role for dysferlin-mediated membrane repair during mechanical stress[14] and extend these observations by demonstrating the importance of membrane resealing as a critical component of the cytoprotective effects of inflammatory signaling after I/R injury. These results are also concordant with our earlier in vitro observations, wherein we demonstrated that TNF-mediated signaling through TNFR1 or TNFR2 preserved sarcolemmal membrane integrity (calcium influx and lactic dehyrogenase release) in isolated cardiac myocytes that were subjected to hypoxia reoxygenation injury.[5]

Although the present study did not delineate the mechanism(s) for the cytoprotective role of dysferlin during I/R injury, it bears emphasis that the exact mechanisms responsible for dysferlin-mediated membrane repair are incompletely understood.[32] Moreover, these studies were conducted ex vivo, which excludes the effects of infiltrating inflammatory cells that could also affect innate immune signaling, Accordingly, it will be important, in future studies, to further delineate the interacting protein partners for dysferlin in MHC-TRAF2$_{LC}$ mice, as well as extend these observations to studies in vivo Finally, we cannot exclude the formal possibility that the deleterious effects observed in MHC-TRAF2$_{DN}$ mice after I/R injury were nonspecific, and were secondary to high levels of expression of the transgene, as has been reported for inert proteins that have been overexpressed in the heart.

Conclusions

The results of this study demonstrate, for the first time, that TRAF2-mediated signaling confers cytoprotection in the heart, at least in part, through upregulation of dysferlin, a calcium-triggered exocytotic membrane repair protein. Although the innate immune system has been implicated in maintaining "barrier function" in the skin, gastrointestinal system, and trachea in vertebrate species,[33,34] these observations have focused predominately on activation of the adaptive immune system by the innate immune system in response to disruption of the epithelial barrier. Our results extend this conceptual paradigm and suggest that one of the important functions of innate immune activation in the heart in response to tissue injury is preservation and maintenance of the physical barrier between the extra- and intracellular environment through enhanced and/or facilitated sarcolemmal repair, thereby preventing calcium-induced activation of cell death machinery, loss of cytosolic constituents vital to cell function, as well as preserving the electrochemical gradient across the sarcolemma that is required for membrane excitability and myocyte contraction. Consistent with this thesis, both gain- and loss-of-function studies have shown that TNF and TNF receptors are required for preservation of epidermal barrier function in mice.[35] This point of view is also consistent with the "danger" model of immunity, which proposes that healthy tissue induces tolerance (eg, preconditioning), whereas unhealthy tissue stimulates the adaptive immune system, which would be activated by release of damage-associated molecular patterns.[36] Given that loss of dysferlin-mediated membrane repair attenuated, but did not abrogate, the cytoprotective effects of TRAF2-mediated signaling, it will be important, in subsequent studies, to determine whether additional plasma membrane proteins that were identified by our screening strategy contribute to maintaining sarcolemmal repair after I/R injury.

Acknowledgments

The authors would like to thank Lora Staloch for technical assistance.

Sources of Funding

This research was supported by research funds from the NIH (RO1 HL89543, RO1 111094, T32 HL007706, and T32 HL007081).

Disclosures

None.

References

1. Brown JM, Grosso MA, Terada LS, Whitman GJR, Banerjee A, White CW, Harken AH, Repine JE. Endotoxin pretreatment increases endogenous myocardial catalase activity and decreases ischemia-reperfusion injury of isolated rat hearts. *Proc Natl Acad Sci USA*. 1989;86:2516–2520.
2. Eddy LJ, Goeddel DV, Wong GHW. Tumor necrosis factor-a pretreatment is protective in a rat model of myocardial ischemia-reperfusion injury. *Biochem Biophys Res Commun*. 1992;184:1056–1059.
3. Mann DL. Stress-activated cytokines and the heart: from adaptation to maladaptation. *Annu Rev Physiol*. 2003;65:81–101.
4. Lecour S, Suleman N, Deuchar GA, Somers S, Lacerda L, Huisamen B, Opie LH. Pharmacological preconditioning with tumor necrosis factor-alpha activates signal transducer and activator of transcription-3 at reperfusion without involving classic prosurvival kinases (Akt and extracellular signal-regulated kinase). *Circulation*. 2005;112:3911–3918.
5. Nakano M, Knowlton AA, Dibbs Z, Mann DL. Tumor necrosis factor-a confers resistance to injury induced by hypoxic injury in the adult mammalian cardiac myocyte. *Circulation*. 1998;97:1392–1400.
6. Nelson SK, Wong GHW, McCord JM. Leukemia inhibitory factor and tumor necrosis factor induce manganese superoxide dismutase and protect rabbit hearts from reperfusion injury. *J Mol Cell Cardiol*. 1995;27:223–229.
7. Lecour S, Rochette L, Opie L. Free radicals trigger TNF alpha-induced cardioprotection. *Cardiovasc Res*. 2005;65:239–243.
8. Kurrelmeyer K, Michael L, Baumgarten G, Taffet G, Peschon J, Sivasubramanian N, Entman ML, Mann DL. Endogenous myocardial tumor necrosis factor

protects the adult cardiac myocyte against ischemic-induced apoptosis in a murine model of acute myocardial infarction. *Proc Natl Acad Sci USA*. 2000;290:5456–5461.

9. Lecour S, Smith RM, Woodward B, Opie LH, Rochette L, Sack MN. Identification of a novel role for sphingolipid signaling in TNF alpha and ischemic preconditioning mediated cardioprotection. *J Mol Cell Cardiol*. 2002;34:509–518.
10. Deuchar GA, Opie LH, Lecour S. TNFalpha is required to confer protection in an in vivo model of classical ischaemic preconditioning. *Life Sci*. 2007;80:1686–1691.
11. Burchfield JS, Dong JW, Sakata Y, Gao F, Tzeng HP, Topkara VK, Entman ML, Sivasubramanian N, Mann DL. The cytoprotective effects of tumor necrosis factor are conveyed through tumor necrosis factor receptor associated factor 2 in the heart. *Circ Heart Fail*. 2010;3:157–164.
12. Yeh WC, Pompa JL, McCurrach ME, Shu HB, Elia AJ, Shahinian A, Ng M, Wakeham A, Khoo W, Mitchell K, El Deiry WS, Lowe SW, Goeddel DV, Mak TW. FADD: essential for embryo development and signaling from some, but not all, inducers of apoptosis. *Science*. 1998;279:1954–1958.
13. Lee SY, Reichlin A, Santana A, Sokol KA, Nussenzweig MC, Choi Y. TRAF2 is essential for JNK but not NF-kappaB activation and regulates lymphocyte proliferation and survival. *Immunity*. 1997;7:703–713.
14. Han R, Bansal D, Miyake K, Muniz VP, Weiss RM, McNeil PL, Campbell KP. Dysferlin-mediated membrane repair protects the heart from stress-induced left ventricular injury. *J Clin Invest*. 2007;117:1805–1813.
15. Sakata Y, Dong JW, Vallejo JG, Huang CH, Baker JS, Tracey KJ, Tacheuchi O, Akira S, Mann DL. Toll-like receptor 2 modulates left ventricular function following ischemia-reperfusion injury. *Am J Physiol Heart Circ Physiol*. 2007;292:H503–H509.
16. Birnbaum Y, Hale SL, Kloner RA. Differences in reperfusion length following 30 minutes of ischemia in the rabbit influence infarct size, as measured by triphenyltetrazolium chloride staining. *J Mol Cell Cardiol*. 1997;29:657–666.
17. Dennis G Jr, Sherman BT, Hosack DA, Yang J, Gao W, Lane HC, Lempicki RA. DAVID: database for annotation, visualization, and integrated discovery. *Genome Biol*. 2003;4:3.
18. Hayter AJ. The maximum familywise error rate of Fisher's least significant difference test. *J Am Stat Assoc*. 2012;81:1000–1004.
19. Divakaran VG, Evans S, Topkara VK, Diwan A, Burchfield J, Gao F, Dong J, Tzeng HP, Sivasubramanian N, Barger PM, Mann DL. Tumor necrosis factor receptor associated factor 2 signaling provokes adverse cardiac remodeling in the adult mammalian heart. *Circ Heart Fail*. 2013;6:535–543.
20. Han R, Campbell KP. Dysferlin and muscle membrane repair. *Curr Opin Cell Biol*. 2007;19:409–416.
21. Ma X, Yang K-C, Liu H, Murphy J, Barger P, Mann DL, Diwan A. TRAF2 coordinates with PARKIN to mediate mitochondrial autophagy in cardiomyocytes. 2013;128:A12198.
22. McNeil PL, Terasaki M. Coping with the inevitable: how cells repair a torn surface membrane. *Nat Cell Biol*. 2001;3:E124–E129.
23. Clarke MS, Caldwell RW, Chiao H, Miyake K, McNeil PL. Contraction-induced cell wounding and release of fibroblast growth factor in heart. *Circ Res*. 1995;76:927–934.
24. Gajic O, Lee J, Doerr CH, Berrios JC, Myers JL, Hubmayr RD. Ventilator-induced cell wounding and repair in the intact lung. *Am J Respir Crit Care Med*. 2003;167:1057–1063.
25. McNeil PL, Kirchhausen T. An emergency response team for membrane repair. *Nat Rev Mol Cell Biol*. 2005;6:499–505.
26. Giraudo CG, Garcia-Diaz A, Eng WS, Yamamoto A, Melia TJ, Rothman JE. Distinct domains of complexins bind SNARE complexes and clamp fusion in vitro. *J Biol Chem*. 2008;283:21211–21219.
27. Cao CM, Zhang Y, Weisleder N, Ferrante C, Wang X, Lv F, Zhang Y, Song R, Hwang M, Jin L, Guo J, Peng W, Li G, Nishi M, Takeshima H, Ma J, Xiao RP. MG53 constitutes a primary determinant of cardiac ischemic preconditioning. *Circulation*. 2010;121:2565–2574.
28. Bashir R, Britton S, Strachan T, Keers S, Vafiadaki E, Lako M, Richard I, Marchand S, Bourg N, Argov Z, Sadeh M, Mahjneh I, Marconi G, Passos-Bueno MR, Moreira ES, Zatz M, Beckmann JS, Bushby K. A gene related to *Caenorhabditis elegans* spermatogenesis factor fer-1 is mutated in limb-girdle muscular dystrophy type 2B. *Nat Genet*. 1998;20:37–42.
29. Rosales XQ, Moser SJ, Tran T, McCarthy B, Dunn N, Habib P, Simonetti OP, Mendell JR, Raman SV. Cardiovascular magnetic resonance of cardiomyopathy in limb girdle muscular dystrophy 2B and 2I. *J Cardiovasc Magn Reson*. 2011;13:39.
30. Wenzel K, Geier C, Qadri F, Hubner N, Schulz H, Erdmann B, Gross V, Bauer D, Dechend R, Dietz R, Osterziel KJ, Spuler S, Ozcelik C. Dysfunction of dysferlin-deficient hearts. *J Mol Med*. 2007;85:1203–1214.
31. Chase TH, Cox GA, Burzenski L, Foreman O, Shultz LD. Dysferlin deficiency and the development of cardiomyopathy in a mouse model of limb-girdle muscular dystrophy 2B. *Am J Pathol*. 2009;175:2299–2308.
32. Cacciottolo M, Belcastro V, Laval S, Bushby K, Di BD, Nigro V. Reverse engineering gene network identifies new dysferlin-interacting proteins. *J Biol Chem*. 2011;286:5404–5413.
33. Feingold KR. Innate immunity stimulates permeability barrier homeostasis. *J Invest Dermatol*. 2013;133:1925–1927.
34. Karrasch T, Jobin C. Wound healing responses at the gastrointestinal epithelium: a close look at novel regulatory factors and investigative approaches. *Z Gastroenterol*. 2009;47:1221–1229.
35. Jensen JM, Schutze S, Forl M, Kronke M, Proksch E. Roles for tumor necrosis factor receptor p55 and sphingomyelinase in repairing the cutaneous permeability barrier. *J Clin Invest* 1999 December;104:1761–1770.
36. Matzinger P. The danger model: a renewed sense of self. *Science* 2002 April 12;296:301–305.